REPUBLIC OF TURKEY

ALTINBAS UNIVERSITY

Institute of Graduate Studies

Electrical and Computer Engineering

A BENDABLE EBG BASED A VIVALDI FRACTAL ANTENNA FOR RF-ENERGY HARVESTING APPLICATIONS FOR 5G NETWORKS

AHMED ABDULMAJEED ABDULHAMED

Doctor of Philosophy

Supervisor

Asst. Prof. Dr. SEFER KURNAZ

Istanbul, 2022

A BENDABLE EBG BASED A VIVALDI FRACTAL ANTENNA FOR RF-ENERGY HARVESTING APPLICATIONS FOR 5G NETWORKS

AHMED ABDULMAJEED ABDULHAMED

Electrical and Computer Engineering

Doctor of Philosophy

ALTINBAŞ UNIVERSITY

2022

The thesis titled A BENDABLE EBG BASED A VİVALDİ FRACTAL ANTENNA FOR RF-ENERGY HARVESTİNG APPLİCATİONS FOR 5G NETWORKS prepared by AHMED ABDULMAJEED ABDULHAMED and submitted on 18/08/2022 has been **accepted unanimously** for the degree of PhD dissertation in Electrical and Computer Engineering.

____

Asst. Prof. Dr. Sefer Kurnaz
Supervisor

Thesis Defense Committee Members:

Asst. Prof. Dr. Sefer Kurnaz	Faculty of Engineering and Architecture, Altinbas University	__________________
Asst. Prof. Dr. Abdullahi Abdu Ibrahim	Faculty of Engineering and Architecture, Altinbas University	__________________
Asst. Prof. Dr. Zeynep Altan	Faculty of Engineering and Architecture, Beykent University	__________________
Asst. Prof. Dr. Oğuz karan	Faculty of Engineering and Architecture, Altinbas University	__________________
Asst. Prof. Dr. Sedar Kargin	Faculty of Biomedical Engineering, Beykent University	__________________

I hereby declare that this thesis meets all format and submission requirements of a PhD dissertation
Submission data of the thesis to Institute of Graduate Studies: ___/___/___

I hereby declare that all information/data presented in this graduation project has been obtained in full accordance with academic rules and ethical conduct. I also declare all unoriginal materials and conclusions have been cited in the text and all references mentioned in the Reference List have been cited in the text, and vice versa as required by the abovementioned rules and conduct.

AHMED ABDULMAJEED ABDULHAMED

ABSTRACT

A BENDABLE EBG BASED A VIVALDI FRACTAL ANTENNA FOR RF-ENERGY HARVESTING APPLICATIONS FOR 5G NETWORKS

AHMED ABDULMAJEED ABDULHAMED

Ph.D, Electrical and Computer Engineering, Altınbaş University

Supervisor: Asst. Prof. Dr. SEFER KURNAZ

Date: /18/08/ 2022

Pages: 88

Radio frequency (RF) based energy harvesting technologies have attracted different efforts from researchers to employ low energy in powering portable electronic devices. In this article, an Ultra-Wide Band (UWB) antenna based a Vivaldi fractal antenna backed with an Electromagnetic Bandgap (EBG) is exemplified for RF-energy harvesting in the modern 5G networks. The antenna is connected to full wave rectifier circuit to obtain a rectified DC current. The antenna is printed on a flexible Kodak photo work of 0.5mm thickness with $\varepsilon r=2$ and loss tangent of 0.0015. The numerical simulations are conducted using CST MWS and HFSS software packages. The proposed antenna structure is fabricated using an ink jet printing technology based on conductive silver nanoparticle ink.

Keywords: Metamaterial, Vivaldi Antenna, Solar Panel, RF harvesting, IoT

TABLE OF CONTENTS

Pages

LIST OF TABLES

Pages

LIST OF FIGURES

Pages

ABBREVIATIONS

MTM	: Meta Material
HFFS	: High-Frequency Structure Simulator
CST	: Computer Simulation Technology
HSR	: H- SHAPE RESONATOR
UWB	: ULTRA WIDE BAND ANTENNA
FIT	: FINITE INTEGRAL TECHNIQUE
PCB	: Printed Circuit Board
RFEH	: Radio Frequency Energy Harvesting
EBG	: Electro Magnetic Band Gab
TEM	: TRANSVERSE ELECTRO-MAGNETIC
S11	: S Parameters
NRI	: NEGATIVE-REFRACTIVE-INDEX
NPV	: NEGATIVE PHASE VELOCITY

1. INTRODUCTION

The last three decades, there has been an increase in scientific interest in the concept of Electromagnetic Band Gap (EBG) structures as photonic band gaps. Recent work have focused on the effects of connecting EBG structures to antenna performance for the purpose of improving their performance [1]. As a metamaterial category, EBG structures are periodic-like layers with outstanding surface wave concealing features, one of which is not observed in nature [2]. EBG constructions were characterized as near zero refractive index [3], soft and hard surfaces [4], high-impedance surfaces [5], and artificial magnetic conductors [6] based on their unconventional electromagnetic properties. A couple of these structures have relative electromagnetic properties [7], which is worth noting. As a result, EBG structures can be thought of as a unique type of metamaterial [8, [9], [10], and [11], having frequency stop bands, passbands, and band gaps in their interactions with electromagnetic waves. [13]. The macroscopic resonance sometime is called Bragg resonance that is relative to the unit cell periodicity; whereas, the microscopic resonance, called Mie resonance, is relative to the lattice resonance [14]. aps.

Another type of EBG structure is the Frequency Selective Surface (FSS), which is stacked as dielectric and/or metallic unit cells in various ways [12]. Such structures are often high-resonant structures that are heavily influenced by the periodicity's macroscopic and microscopic resonances. [16].

FSS classifications have recently been established as filters [17], artificial magnetic conductors [18], photonic crystals [19], and photonic band gaps [20] based on their applications. Furthermore, these structures can be employed as artificial periodic and non-periodic layers to prevent and/or aid the propagation of incident waves [21]. In both TE and TM, the structures have a high impedance mode as found in mushroom-like structures [22], in which, an in-phase reflection coefficient can be created [23]. Moreover, soft and hard surfaces operate as FSS structures [24]; which are included in a wide range of applications in the antenna engineering researches and industries.

1.1 BACKGROUND

The metamaterials have features that go beyond the properties of naturally materials. The name is derived from the Greek word "meta", which means beyond nature, these materials are built artificially with a certain specifications to achieve the required performance. Their properties are due to the structural composition and not physical composition [1]. Metamaterials can be defined as the material that gains its EM properties from the material structure rather than the material itself. If the structure is precisely engineered a negative refractive index can be obtained at certain frequencies. In other words, these materials are not subject to the right-hand rule, hence the name "left -handed MTM" [2].

The negative refractive index does not mean the permanent movement of the signal, but rather the bending of electromagnetic waves in the opposite direction when they cross from a RH-medium to a LH-medium as shown in Figure 1.1[3].

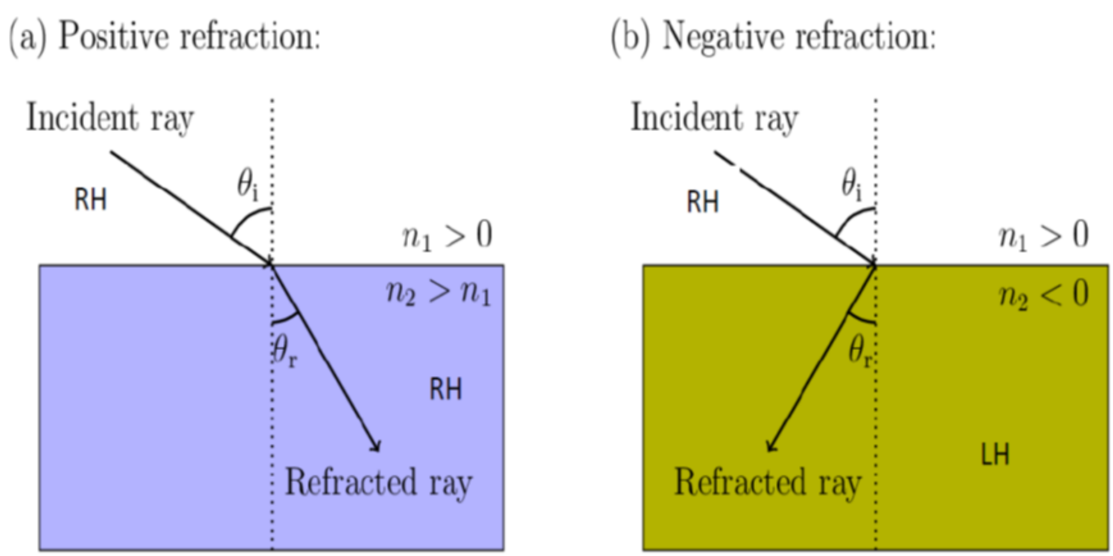

Figure. 1.1: Electromagnetic wave refraction at the media interface. (a) Two mediums of similar handedness (positive refraction), (b) two mediums of opposite handedness (Negative refraction)

The metamaterials are considered a rich material for researchers and scientific research and cover a wide range of frequencies extending from radio waves to the visible range [4]. In recent years, the use of these materials has extended to the microwave frequency range (1-100 GHz), more details will be given in section 1.8 about MTM applications.

1.2 MTMS AND LH- MTM DEFINITIONS

The metamaterials can be defined as an effective homogeneous artificial materials with properties and characteristics not found in nature [5]. The effective homogeneous structure is a material that its cell size p is very small compared to g is the guided wavelength The average cell size must be smaller than a quarter wavelength p g/4 for this to work., To ensure the dominance of the refraction phenomenon over the phenomenon of scattering / diffraction during the propagation of electromagnetic waves in the middle of a MTM. The condition [p = λg/4] will be considered as the condition of effective homogeneity [6]. The parameters [$\varepsilon r\ \mu r$] depend on the properties of the unit cell as the construction becomes a real material in the case of effective homogeneity, and as a result the structure is considered to be electromagnetic uniform in the propagation direction. The refractive index n can be determined by the structure's constitutive parameters, permittivity and permeability, are given by the following relationship:-

$$n = \pm\sqrt{\varepsilon r\ \mu r} \ldots\ldots\ldots\ldots\ldots\ldots(1.1) \qquad (1.1)$$

0 =/r = 8.854 * 1012, 0 =/r = 4 *107, where r and r are free space relative permittivity and permeability, respectively. Figure 1.2 represent the ε− μ diagram which shows the sign combinations for the (ε,μ) pair . Which are (+,+), (+,−), (−,+), and (−,−),Where the first three groups are known in the traditional materials, while the fourth group is the new type, which is referred to as LH- materials [7]. As a result of the negative sign of the constitutive parameters, the LH-MTM has antiparallel phase and group velocities. According to the previous definition, LH materials are considered metamaterials because they are artificial (man-made) and effective homogeneous (p <λg/4), in addition to the unique properties (εr , μr < 0). The term MTM has been used to refer to LH-materials in references, but it includes a much broader scope.

Perhaps LH-materials are the most common type of meta materials due to their distinctive properties with a negative refractive index. This chapter focuses on this class of meta materials, namely composite right/left-handed CRLH meta materials..

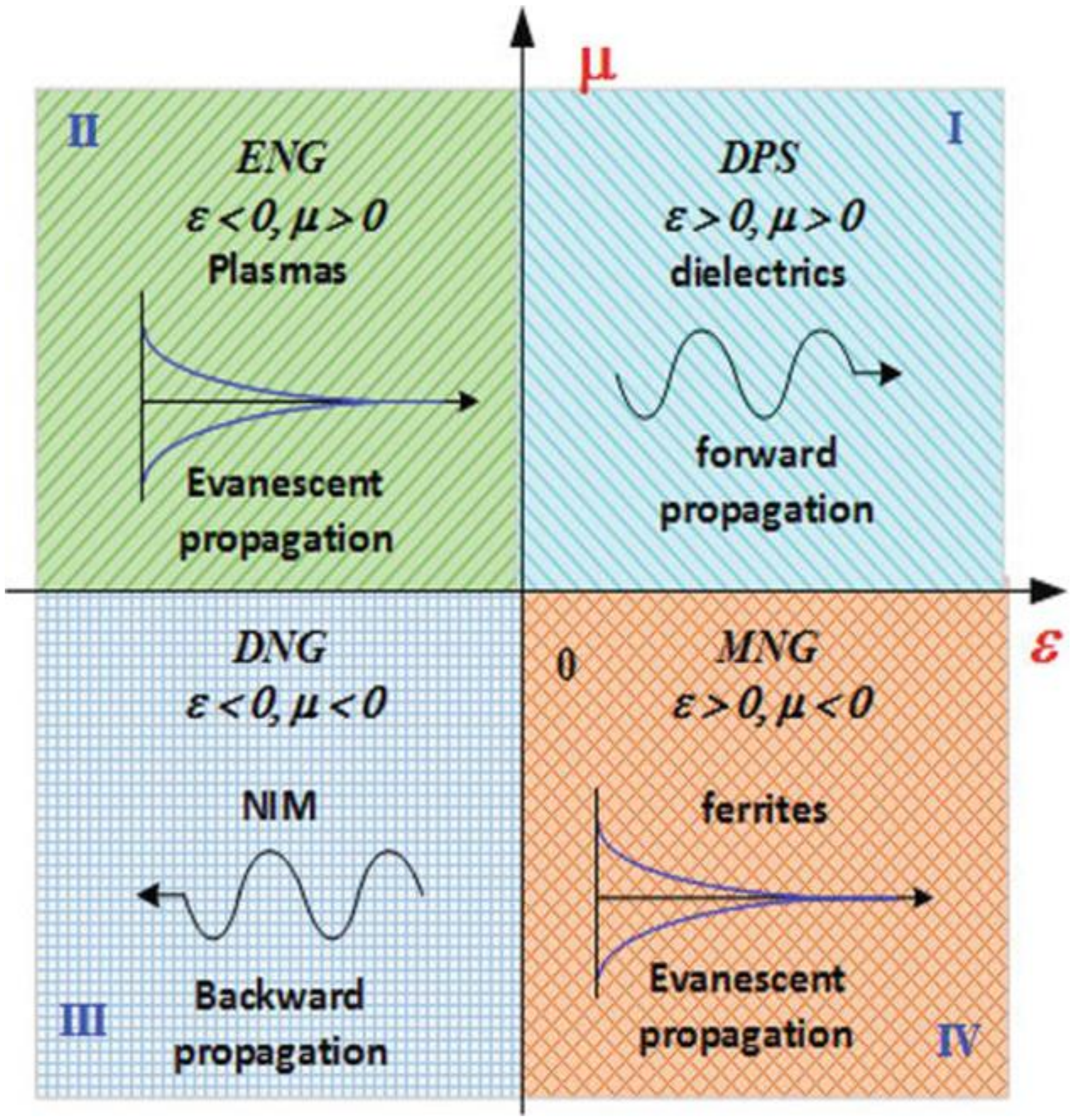

Figure. 1.2 : The (ε − μ) diagram [8]

1.3 VESELAGO THEORY

The emergence of the metamaterials return to 1967 with the theory of the Russian scientist that explain the existence of materials with negative constitutive parameters (ε & $\mu<0$) [9], the fourth quarter in fig 1.2. Veselago called these structures LH- materials because they allow electromagnetic waves to propagate and form a left-handed triangle with both, the electric and magnetic field along with the phase constant vector, which is different from traditional materials that form a right-handed triangle. Veselago predicted various abnormal physical phenomena that occur in association with LH- materials:-

a. The constitutive parameters are frequency disperitive.

b. The reverse of Doppler shift.

c. The Reverse of Cherenkov radiation.

d. Reverse the boundary conditions relate the electromagnetic wave components at the interface between LH/RH materials.

e. The reverse of refraction law (The law of Snell)

f. The law of Snell Negative refraction at the edge of the medium that separates RH and LH mediums.

g. Using an LH slab, a point source can be converted into a point picture..

h. Reverse of the convergent and divergent effects in LH- lenses.

y. In resonant LH materials, the () parameters have a plasmonic impact.

Veselago concluded his research by describing "substances that may demonstrate left-handedness" that are genuine (natural). He speculated that LH could be "plasma and magnetic gyrotropic molecules." where both ε and μ have negative signs. Nevertheless, Veselago expressed his sadness with the lack of an isotropic substance with a negative permeability, which indicates the difficulty of achieving a LH- structure. No substance of LH- structure was detected at that time

1.4 THE DIFFERENCE BETWEEN BACKWARD WAVES AND LH-MTM.

Antiparallel phase and group velocity propagation have been known for a long time in various fields and it's not a new theory. The circuit model shown in Figure 1.3 was used by Brillouin and Pierce to represent the CRLH model and its multiple uses, and is used specifically to describe this type of propagation, signals with such characteristics are called backward waves [10].

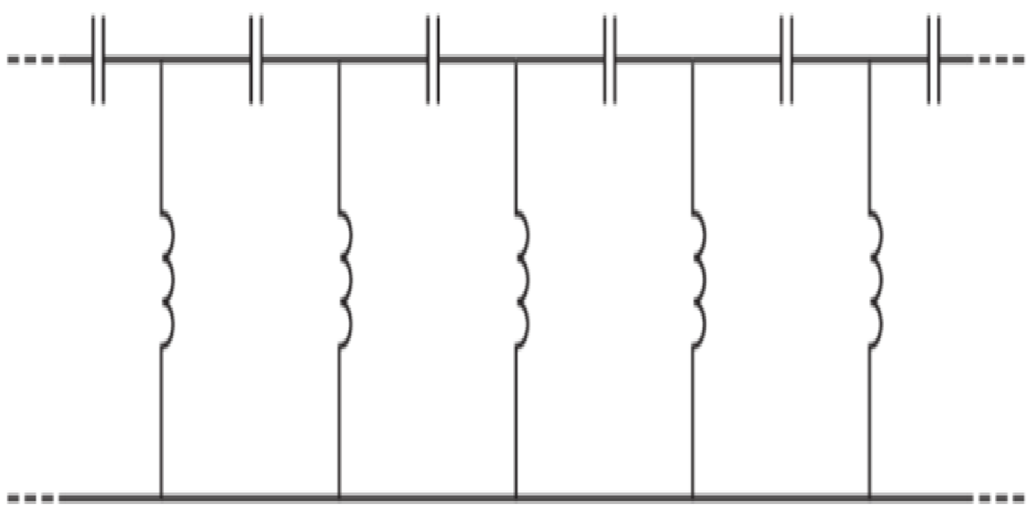

Figure. 1.3: A circuit model for backward wave line

Backward waves have been associated with the phenomenon of reverse amplification in traveling wave tubes, there are many references that explain in details the backward waves, for all cases of the background wave's phenomenon except for the magnetostatic backward volume waves, these waves occur at space harmonics or at higher modes. Therefore, in structures where this type of wave propagates, the cell size must be equal to half the wavelength (p g/2) or several wavelengths (p ng/2) at the higher modes. As a result, diffraction and scattering phenomena dominate the structures through which these waves propagate and therefore cannot be described by the parameters ε and μ[11].Thus it will not present the electromagnetic behavior of real structures, for example the property of refraction subject to Snell law. On the other hand, LH-MTM operate at the fundamental mode, effective homogenous structure where the cell size is smaller than $\lambda g/4$, hence the constitutive parameters can be identified and the structure behave as a real material.

In reality, as long as the cell size is less than quarter wavelength $p < \lambda g/4$, the distinction between left handed structures and dielectric materials is just quantitative. The structural units producing a particular permittivity value in natural dielectric materials are constitutive molecules of the order of the Angstrom, whereas in contemporary left- handed materials it has a volume of centimeters in the microwave region. The electric size of the unit structure is equal to $p/\lambda g \approx 10-9$ in the L-X microwave bands for the first case and equal to $p/\lambda g \approx 10-1 - 10-2$ for the second case. However, LH MTMs exhibit qualitatively identical refractive phenomena to conventional dielectrics. This is where the essential uniqueness of LH-MTMs lies: LH-MTMs are artificial structures that behave similarly to dielectrics, thus the name materials in metamaterials, but with negative properties. Because of their effective homogeneity, LH MTMs may be expanded to 2D and 3D structures.

1.5 TERMINOLOGY

There is currently no agreement on nomenclature for MTMs, Several comparable terminology have been used, each with merits and disadvantages:

a. This is the name mentioned by Veselago and is considered closely related with the most important feature represented by antiparallel phase and group velocities ,in addition of being suitable for structures with different dimensions [12] . Some scientists consider this term to be misunderstood with left-handed chiral materials, which represent shortcoming of this name.

b. Double-negative (DNG) - The aforementioned potential misunderstanding is not conceivable in this situation. However, what is negative is not determined and as a result it is not considered ideal

c. Negative-refractive-index (NRI) -NRI is a relevant word for 2-D and 3-D construction, and it also emphasizes the essentially homogenous character of LH MTMs. It loses its meaning in one-dimensional structures due to the non-participate angles of propagation.

d. Backward-wave (BW) -The advantage of this name is that it indicates the presence of antiparallel phase and group velocities, which are widely recognized in conventional materials, but it failed to enlighten on the structure (effective homogeneous) character of LH -MTMs.

e. Veselago medium -This option pays homage to Veselago's innovative notion but does not give any information about the medium's characteristic.

f. Negative phase velocity medium (NPV) - this name is the finest of all in terms of semantics, but is so rare in use that it may be too early to accept it definitively, Unless it is agreed between MTM Research Eminent Persons to use it. Left-handed (LH) MTM will be used in this chapter.Second paragraph.

1.6 COMPOSITE RIGHT/LEFT-HAND (CRLH) MTMS

Caloz proposed the idea of CRLH-MTM, which represents represents the broader case of LH MTMs and provides a short description of the core.

The TL model in Figure 1.4 is made up of series [interdigital] capacitors CL and shunt [stub] inductors LL, which are supposed to provide left-handedness from the previous model. section's clarifications. However, currents and voltages produce parasitic effects when they pass through the material. [13].

When current is passed through the capacitor CL, a magnetic field is generated, resulting in a series inductance LR; moreover, voltage gradients occur between the upper conductors and the ground plane, resulting in a shunt capacitance CR. As a result, even in a limited frequency range, a pure LH (PLH) structure is not completely present, because a true LH structure must incorporate (LR,CR) and (LL,CL) reactance. This fact is the basis for the use of the name CRLH to explain the properties and nature of actual left handed- MTM [14].

The basic features of a CRLH may be deduced from an examination of the analogous model shown in Figure 1.9. (a) , LR and CR are short and open at low frequency range, therefore the circuit become pure LH-structure This LH is unique in that it possesses antiparallel phase and group velocities. structure is high pass circuit, so an LH stopband is present below a certain cutoff. While at high frequency range CL and LL are short and open. The circuit become purely RH- structure with parallel phase and group velocities, this RH- structure is low-pass circuit, so an RH stopband is present above a particular cutoff. Generally, when the series and shunt resonances are not equal, gap is exist amongst LH and RH structures.

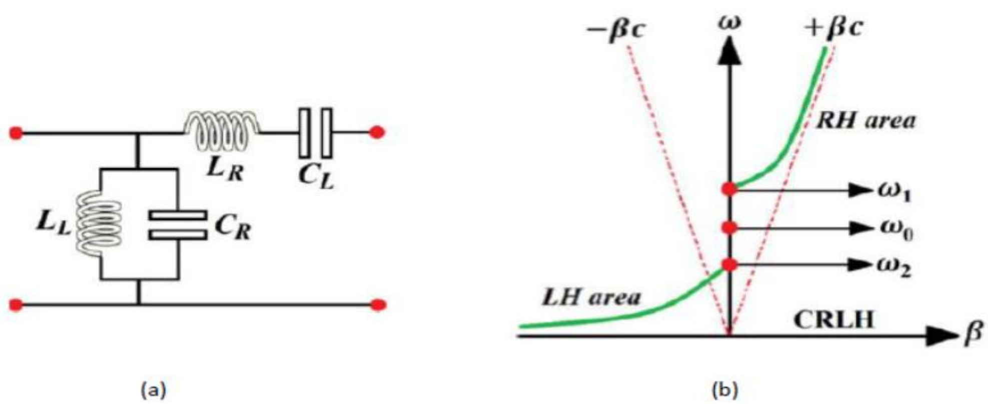

Figure. 1.4: CRLH- MTMs characteristic. (a) Unit cell structure (b) Dispersion diagram.

(LR = CR = 0 at LH circuit), (LL = CL =∞ at RH circuit) Mentioned for comparison purposes. In this diagram ωse < ωsh , the opposite can be applied also depending on the LC values. If the resonances are balanced, the gap is completely disappear, as well as a wave length that is infinite propagation (λg = 2π/|β|) at the frequency of transition ω0 is obtained. Despite the filter feature, CRLH operated only at the transition frequency where the condition of effective homogeneity is satisfied (p < λg/4), it never operate at the borders the Brillouin zone, a p ≈ λg/2. The dispersion curve in the CRLH containing LH and RH effects is quite different from the pure LH/ RH structures due to the combined effect of the structures at all frequencies.

1.7 THE IMPLEMENTATION OF CRLH- MTM USING LC NETWORK

As previously stated, a purely LH structure cannot exist even with a circuit containing only a series capacitance and a shunt inductance, this is due to the parasitic effects of the shunt capacitance and series inductance that result from the flowing of current through the metal and the voltage developed between the metal and the ground[15],[16]. Accordingly, the CRLH structure represent the general form of this type. Figure 1.5 shows a structure for the CRLH loss-less case. The model consists of an impedance Z(Ω/m) represented by LR (H/m) in series with CL (F•m), in addition to admittance Y(S/m) represented by CR (F/m) parallel with LL (H•m), all the parameter are per unit length [17].First paragraph.

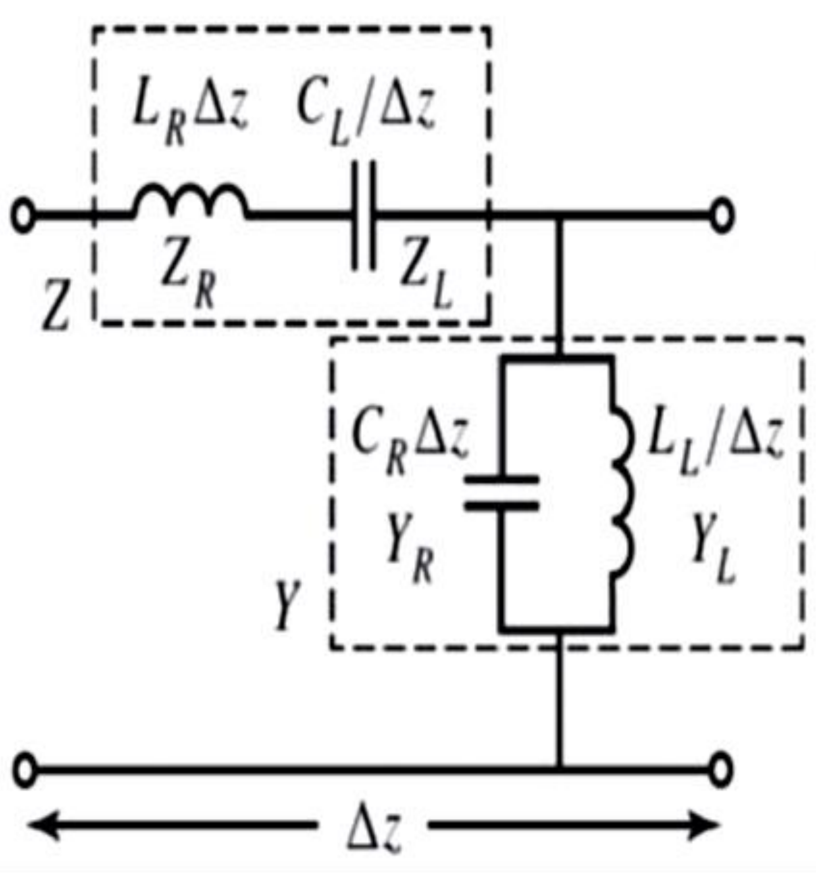

Figure. 1.5: Model of the ideal CRLH TL's equivalent circuit

The previous ideal CRLH structure is not actually available, but rather an effectively homogeneous structure within specified frequency range can be built based on a ladder network [18]. This network can be obtained by sequentially connecting the cell shown in Figure 1.6 to produce the ladder network shown in Figure 1.7, the unit cell structure consist from an impedance Z=LR+CL in series with an admittance Y= 1/CR+1/LL. in the balanced case, the series and shunt resonances are made equal so that no gap is exist between the LH and RH regions in the CRLH TL line.

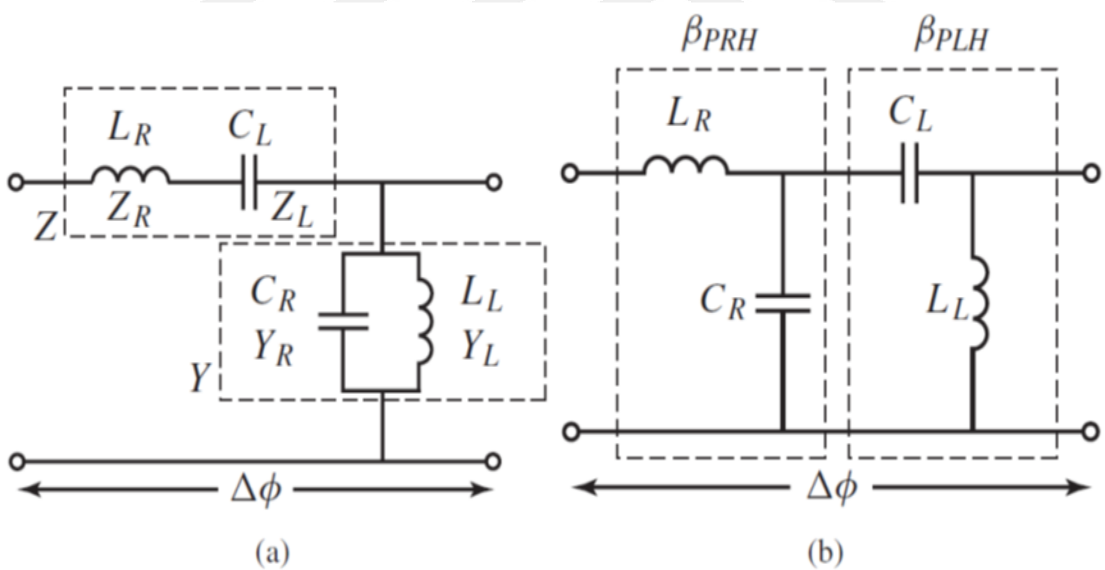

Figure. 1.6: LC CRLH TL unit cell structure. (a) Unbalanced case (b) Balanced case

(LRCL = LLCR).

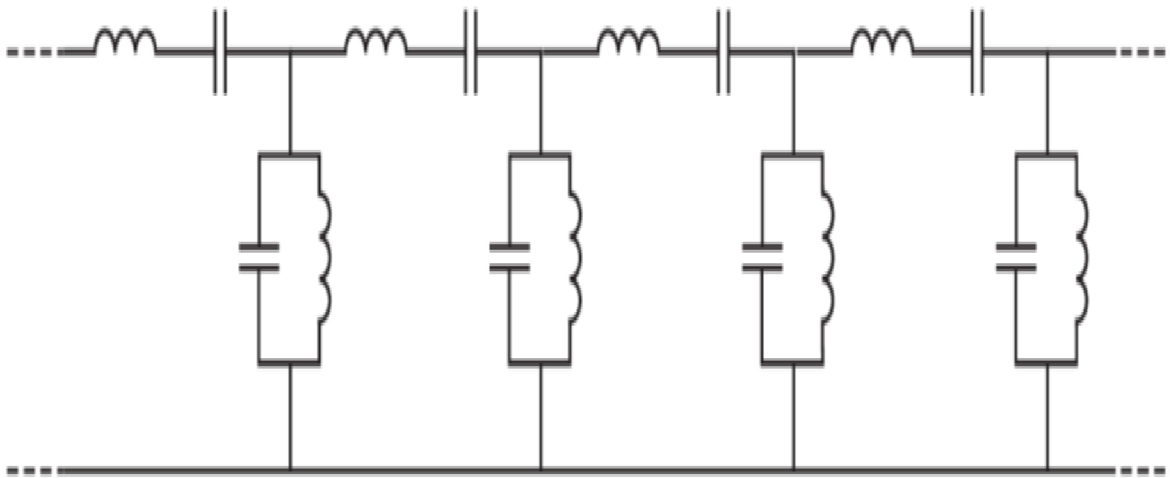

Figure. 1.7: The construction of Periodic ladder network based unbalanced LC CRLH- TL.

When p= Δz → 0, then immittances per unit length becomes Z/p Z, Y/p Y, Z/p Zthus the L-C circuit of Fig (1.6/a) becomes identical to the circuit of Figure 1.5

Figure 1.5 represents a subsection of the transmission line with a length equal to Δz , Practical transmission line of length l can be configured by making copies of this section, where it becomes l= N*Δz.

By connecting the unit cells sequentially as shown in Figure 1.7 and under the condition p → 0, a transmission line identical to ideal CRLH can be obtained with a total length equal to l, as shown in Figure 1.8. This condition is called the homogeneity condition where the artificial transmission line is equal to the loss-less homogeneous line. Actually, this condition could be translated into effective-homogeneity condition, $p < \lambda g/4$ where it prevents the occurrence of resonances along the line discontinuities [19]. The LC construction of CRLH TL represent a band pass filter , since it gather the LH and RH filter behavior explained in previous section, also it show the CRLH behavior represented by the propagation constant β and characteristic impedance Zc, in its passband.

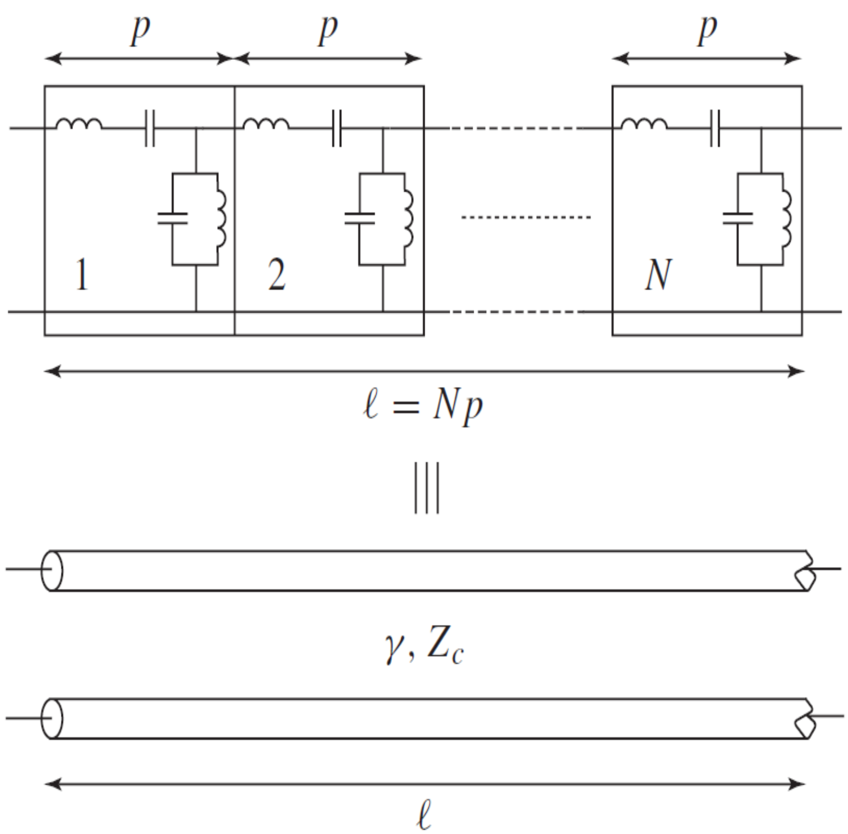

Figure 1.8: periodic ladder network equivalent to an ideal transmission line at the condition $p = \Delta z \rightarrow 0$, at $p< \lambda g/4$ the network structure provide in a bounded frequency extent a good approximation for the ideal TL

1.8 1DISTINCTION FROM CONVENTIONAL FILTERS

Because CRLH TLs may appear similar to ordinary filters at first glance, let us now highlight the key differences among these classes:

A LH-MTM structure has a distinct phase response, resulting in LH transmission a low RH transmission and frequencies at high frequencies. Filters that are commonly used are often built to satisfy magnitude requirements and lack an LH range.

a. An MTM structure is designed for use as a transmission medium .Only the passband has any direct application. Stopbands are often parasitic effects that restrict the MTM's operational bandwidth. As a result, unlike filters, the network's filtering characteristics are rarely employed in MTM.

b. The metamaterials consist of cells that fulfill the condition of homogeneity $|\Delta\varphi| < \pi/2$, while the filters do not necessarily fulfill this condition. The metamaterials possessed $|\Delta\varphi| << \pi/2$, or $\Delta z << \lambda g/4$, are ideal materials, similar to ordinary dielectrics, which are composed of molecules with diameters several orders of magnitude smaller than wavelength. The reason Δz approaches $\lambda g/4$ in some MTM at certain frequencies is due to the lack of more effective materials.

c. The metamaterial extends to two and three dimensions and acts as a bulk medium, while traditional filters are limited to one dimension and act as electrical circuits.

d. The metamaterials are made from similar cells, while in filters the cells have different values to suit a certain criteria.

In response to the last point, metamaterials do not require periodic cell repetition, the repetition process came from a convenience point rather than physics point. In terms of manufacturing, designing a unique cell periodically is much easier than designing cells with different shapes. Mathematically, the use of a uniform structure will make it possible to use theories of periodic structures that are easy and clear, while a non-uniform system will be difficult to analyze mathematically. The insignificance of periodicity in metamaterials is demonstrated by the presence of the ideal transition line. This line is non-periodic and gives unique mode as shown in Figure 1.4. This is the basic mode in the LC periodic network structure, when the periodicity disappears, the different harmonies disappear, leaving only this operating mode. To understand this theory, at the case(p)equals zero, all harmonics shift outside at high frequencies the required band, leaving only the basic harmonic.

1.9 METAMATERIAL APPLICATIONS

Metamaterials provided alternate and unexplored views as a result of their unnatural interactions with the EM waves, overcoming the inherent limits of traditional and sophisticated technology. As a result... it was able to reexamine the principles of electromagnetism from a different perspective, which resulted in:

a. Discovering novel characteristics of electromagnetic materials.

It is increasingly usual to consider metamaterials as materials having negative refractive index, negative permeability, negative permittivity, with very low or very high values of permittivity and permeability. [20].

b. Use of Metamaterials in the implementation of RF components

Metamaterials have the potential to have a substantial influence on sensor technology. These elements primarily consist of active power amplifiers and couplers, power dividers, and bandpass filters (BPFs) as passive circuits [21].

c. Overcoming the inherent constraints of traditional materials

MTM TL are artificial lines with reactive materials that have a larger degrees of freedom than traditional lines and tune both dispersion and characteristic impedance qualities [22].

d. Enhancing the capabilities of current devices

Metamaterials have been effectively employed to increase the performance of previously existing components (for example, in microwave designs) or to create theoretically novel devices such as invisibility cloaks, transformation EM devices, and optical Nano-circuits [23]

1.10 AIM AND CONTRIBUTION OF THIS WORK

In this work there are several contributions to be stated:

a. A new microstrip antenna layout is presented for applications that can be worn.

b. The suggested antenna's basic constituent is a fractal supported by square pads of an EBG array.

c. To demonstrate the design technique and execution of the suggested antenna, extensive numerical analyses are presented..

d. The solar panel's manufactured prototype is made of SNP and tested by experiments being compared to the simulated findings.

e. The antenna shape will be comparatively miniaturized with small dimension.

f. For RF energy harvesting, the suggested antenna has a distinguished gain bandwidth product across a wide frequency range.

g. In terms of receiving and sending in low-energy appliances, the antenna has a smoothly property that makes it ideal for UWB applications..

h. The antenna structure wills be suitable for bending for wearable applications.

The aim of suggested design is to maximise the antenna. bandwidth in which |S11|<-10. The substrate of antenna is considered Kodak photo work of 0.5mm thickness (h) and $\varepsilon r=2$ with $\tan\delta=0.0015$ on area of 32mm×28mm. A 50 feed line is linked to a Vivaldi fractal patch printed on the Kodak substrate in the proposed system. Although the antenna design is based on an equilateral triangular patch, it offers low bandwidths across many frequency bands [6]. As a result, a partial ground plane [12] is proposed to provide considerable bandwidth increase by decreasing surface wave diffractions at ground plane edges. The suggested ECFCPW is designed to maintain a continuous connection between the SMA port and the patch while maximizing the matching bandwidth [18]. To increase antenna bandwidth, curved matching circuits are used [4].

This idea is further modified by putting triangular gaps on the patch to produce new resonance modes by extending the patch's surface current routes [16]. The patch's surface electrical area is then enlarged within the same physical region. The proposed antenna is connected to shorting plates that serve as matching circuits for the planned ECFCPW [12]. Finally, EBG-defects are added to the partial ground plane (see Figure 1.9) to improve antenna matching with good improvements in antenna directivity, gain, and beam-width due to the suppression of surface waves [3]. These EBG structures on the ground plane are defected as square pads to enhance the tangential component of the electric field and the antenna radiation efficiency [9]. Now, the dimensions of the patch structure are realized analytically based on solving the Chebyshev exponential following equation [1]:

$$\boldsymbol{\Gamma} = \frac{1}{2}\int_{z=0}^{L} e^{-2j\beta z}\frac{d}{dz}\ln\left(\frac{z}{Z_0}\right) \quad (1) \tag{1.2}$$

$$f\_r = 0.26\ c/h\_e\ \ 2\text{^}n(2) \qquad (1.3)$$

$$h\_e = (\sqrt{3})/2\ [S + t(\varepsilon\_r\ )\text{^}(-0.5)\ ](3) \qquad (1.4)$$

where, c is the light speed S is the patch side length, t is the thickness of substrate material, and εr is the substrate dielectric features. Hente, according to equation (2), the designed antenna must the leading frequency resonance is 2.34GHz at a fractal index n=2

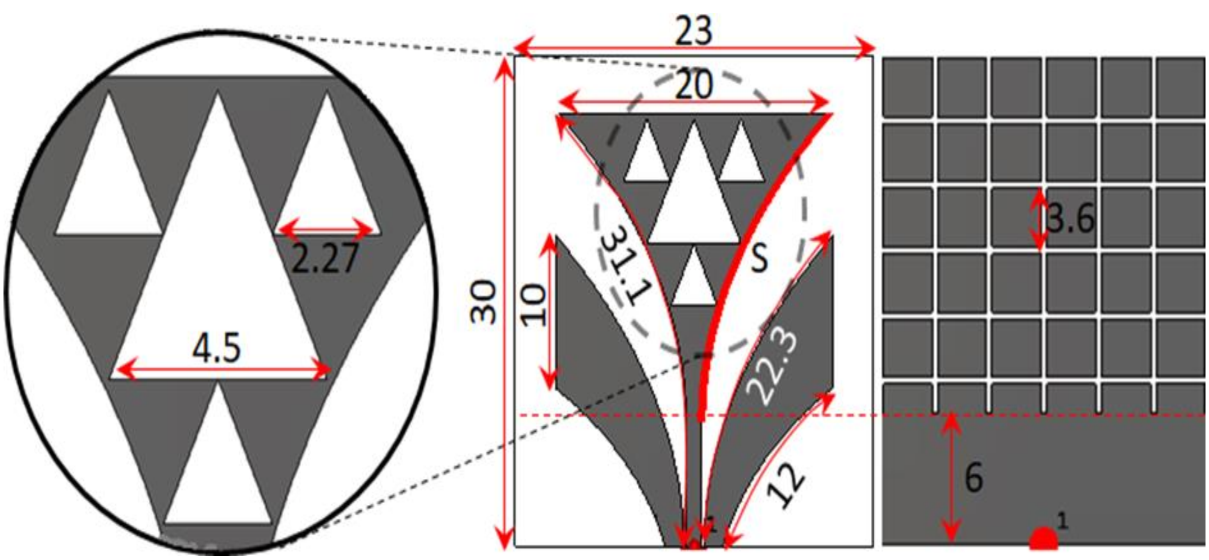

Figure 1.9: The recommended antenna's construction based on the computed dimensions.

1.11 COMPARISON

Table 1 shows the results.antenna achievement will be in comparison to previous literature-based findings. It must be that In terms of size reduction, the suggested desgin outperforms existing published designs.. Such heightening will be as a result of the EBG faults being added that causes the radiation pattern to widen. It aids in energy collecting from various angles. The suggested design differs from past comparable designs it combines tow energy sources based on RF and solar in a one only unified printed circuit.. Therefor the elastic solar panel implementation introduces a new capability to make antenna to fit a lot easier to build wearable and smart apparel.. Nonetheless, a suggested design delivers good frequency matching and adequate gain for Wi-Fi, Wi-Max, and WLAN applications. Moreover, the In compared to different published data, the suggested design produces the least amount of spectrum regarding the solar panel.. Finally, even when, positioned near to the human body, the suggested antenna: has an adequate ability to maintain perfect matching.

.

Table 1.1: Achieved results with respect to published results

References	**Size (mm^2)**	***f* /GHz**	***G*$_o$/dBi**	***V*$_{out}$/V**	**η**
5	32×28	2.45	1.9	0.0022	0.80
17	70×42	2.45	6.2	3.1	0.83
19	32×28	2.45	2.2	2	0.80
19	32×28	5.8	2.48	2.5	0.91
3	180×150	2.45	7	11	0.65
4	200×200	2.45	9	7	0.66
20	180×180	2.45	6	0.35	---
21	160×160	4.14	3.2	0.82	---
22	384×64	3.8	11.6	7	---

1.12 SIGNIFICANCE OF THE STUDY

a. It will be possible to increase the antenna bandwidth and gain for receiving multiple frequency bands. while lowering, the shadowing impact of the patch layer, on the substrate, by using an ultra-wide band patch antenna based, on fractal geometry comprised, of met material structure.

b. The antenna will be designed and simulated using different commercial software packages including CST MWS and HFSS,

c. Perform the related electronic circuits including the A/D converter, the battery charger, the matching circuits and amplifiers,

d. Fabricate the antenna structure and integrate it into the related electronic circuits then test the performance,

e. Measure the harvested power in real outdoor environments.

1.13 SCOPE AND LIMITATIONS OF THE STUDY

The suggested work is confined to the fractal geometry antenna design that will be coupled to the RF harvester at 915MHz in the future. To achieve the antenna performance, the design of the suggested antenna is explored using CST MWS (Computer Simulation Technology based Microwave Studio) using Finite Integral Technique (FIT). Despite this, the antenna was created using the Minkowski fractal of circular shape within a triangular construction.

1.14 ORGANIZATION OF THE THESIS

My thesis consisting of five chapters. Chapter 1 investigates also analyses numerical studies a photovoltaic technology impact on integration of the microwave terminals as described in Chapter 2, with the focus on met materials and antennas separately. In this work, the electromagnetic characterisations of the met material structures are the method used to compute permeability, and relative permittivity, which are investigated. Nevertheless, the antenna in terms of productivity a single terminal is evaluated. Chapter 3 investigates the implementation of the antenna structure according to met materials. The effect of the antenna array with and without met material structure is developed to realise the optimal antenna performance with regard to bandwidth and gain enhancement. The integration and fabrication of the antenna structure based on met material structure is shown chapter 4The research comes, to a close in Chapter 5. and makes recommendations for future related work to be considered.

2. MICROSTRIP OPERATION AND TECHNOLOGY

2.1 MICROSTRIP PATCH ANTENNAS

Microstrip antennas and arrays have piqued the interest of researchers and engineers, and they are widely employed Antennas come in different sizes and shapes, and they are used in radio frequency and microwave systems, such as communications, navigation, and others Patch, dipole, slot, or traveling-wave are examples of these types of antennas. structures, and are intended for specific purposes[1, 2]. Figures 2.1 and 2 show several examples (a-c)

Patch or patch-like radiators have distinct properties that have been well researched. They provide numerous significant benefits:

a. A low profile. Micro strip patch design antenna typically has a thickness of fewer than 0.03 λ (λ is the power wavelength in free space [3].

b. Lightweight. Antennas are made of electrically conductive patch materials such as (PEC) and connected to electrical insulators.

c. Conformability Antennas compatibility consists of a flat or uneven surface, this compatibility can deal with the surface of the insulators to which they are connected.

d. Low price. A microstrip patch antenna was often made using a low-cost printed circuit method. a substrate, is typically the most expensive component of an antenna.

e. Interconnection with: different circuits A microstrip patch antenna may be easily integrated with other planar circuits on a printed circuit board (PCB)[4].

f. Flexibility. By varying the form and feeding arrangement, a microstrip patch antenna may be highly adaptable in (impedance) (resonant frequency) (radiation pattern) (polarization,) and

(operating mode). There are several methods, including short screws and unsteady diodes, as well as loading and slitting the patch. These methods are used to modify the antennas and insert components into the antennas[5].

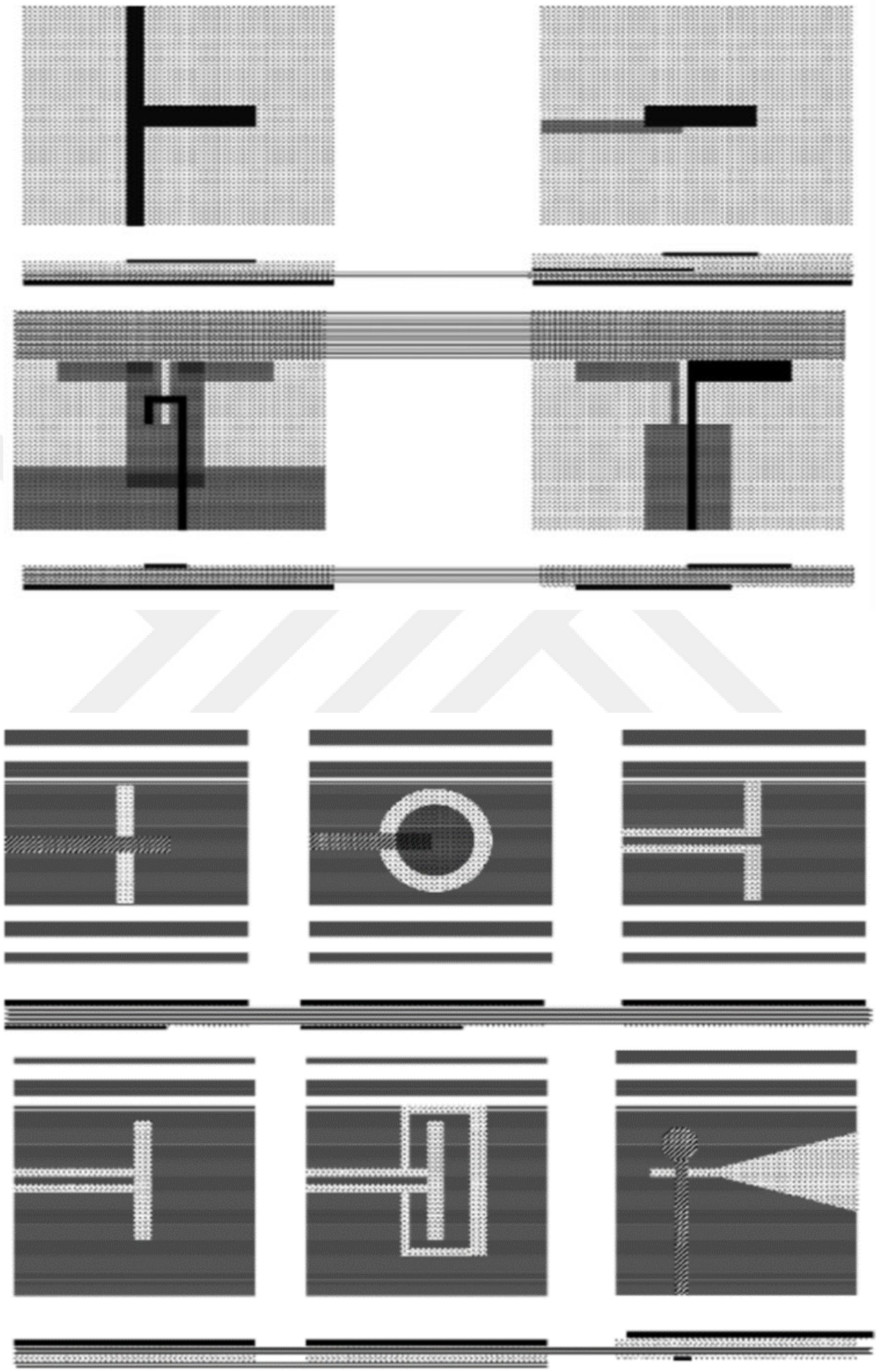

Figure 2.1: (a) dipole, (b) slot, (c) traveling-wave

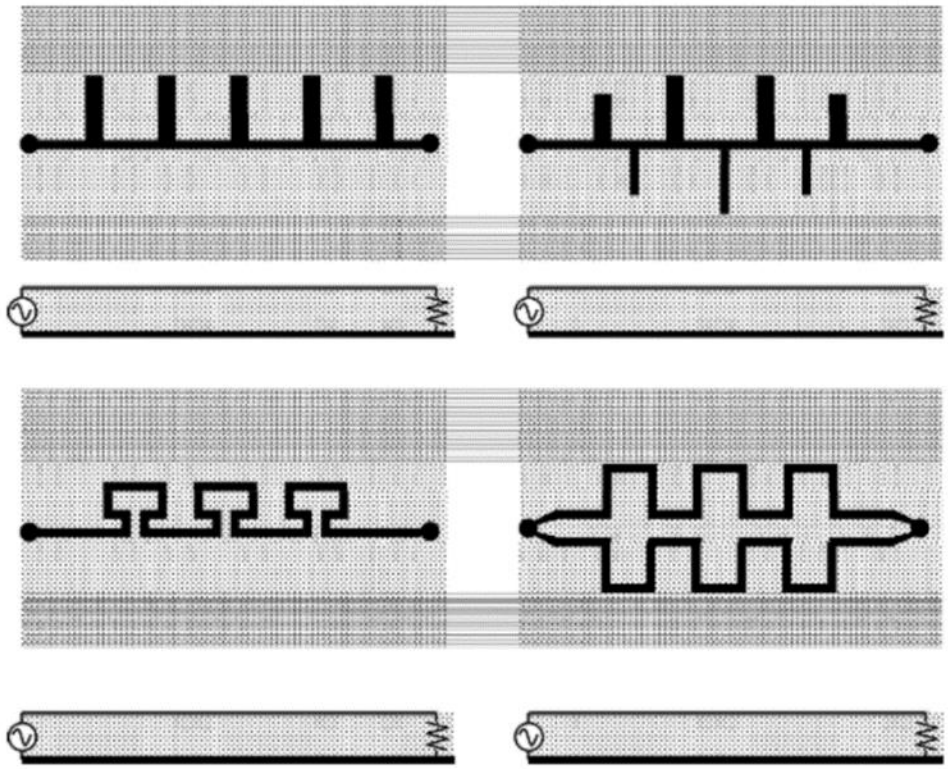

Figure 2.1: (a) dipole, (b) slot, (c) traveling-wave (continue)

However, basic microstrip patch antennas have significant disadvantages. These include a small impedance bandwidth (usually approximately 1%), it will cause lower power capacity, poor scan management, and the radiation efficiency is very low[6]. The principal drawbacks are limited impedance and radiation bandwidths, which are produced mainly through to determine the quality of antennas that can be manufactured by Several factors, the most significant of which is the efficiency a multimeter on frequencies, radiation direction, and polarization. As a result, significant work has been given to developing broadband methods, as highlighted[7].

The raise the frequency bandwidth of antennas are discussed in this chapter. To begin, the fundamental characteristics of these antennas were briefly examined. Following a brief description of broadband methods, an Antennas can be applied in several forms, including direct or with simple changes to form rectangular antennas to know the actual impedance and radiation properties

2.2 KEY PROPERTIES OF MICROSTRIP PATCH ANTENNAS.

As illustrated in Figure 2.2, It shall be a thin, electrically grounded insulating metal layer etched on a substrate[8]. The substrate is too small, less than 0, the correction element is generally used inconsistently with the non-parallel feeding. Patches have significant dimensions of the equivalent wavelength is e arranged on the equation e/2. The radiation pattern was determined by the distribution of electric currents apatch. (patch structure), (feeding) and (substrate) characteristics may be selected to obtain the required performance for, given application[9].

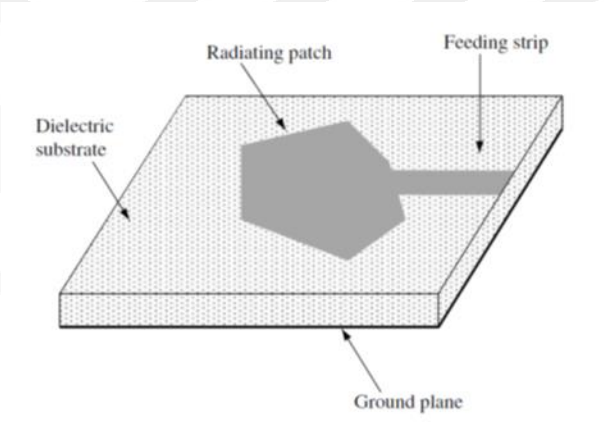

Figure 2.2: A microstrip a radiator

2.2.1. Patch Structure

It is recommended that the radiator be made a low-ohmic-loss, high-conductivity material at the working frequency: (such as copper) and can be attached to Insulation substrate. The form might be a standard rectangle, square, elliptical, triangles circles, ring, pentagon, or variants; F, 2.3 depicts various standard radiators[10]. More sophisticated variants on the fundamental forms were commonly utilized to fulfill specific design requirements. The choice of a certain form is based on a set of criteria. like (polarization), (bandwidth) and (gain). In general, the excited operating modes establish the antenna's properties, which were determined by the form and size a thickness of the radiation element, and the substrate's dielectric fixed. And feed configuration [11].

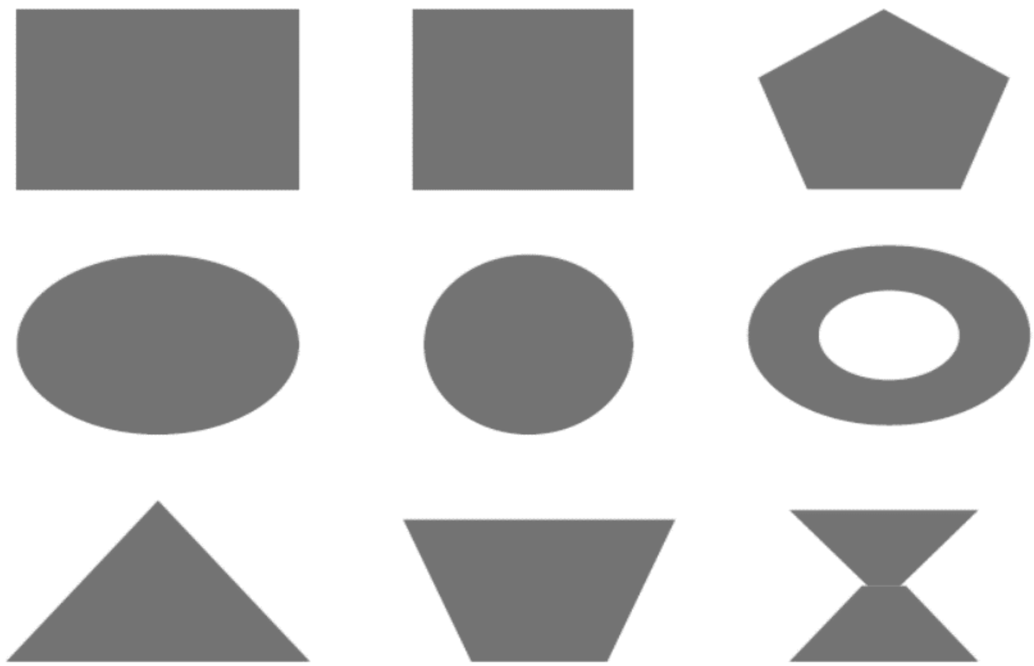

Figure 2.3: geometric of radiators

2.2.2 Substrates

Substrates may be made from a wide range of dielectric materials. A ,dielectric constant (2 2. r 16) in RF or microwave, bands. the dielectric loss tan (0 0001tan 0_06), an imaginary portion of the dielectric (constant), and (cost) are all crucial elements to consider. In the radio frequency and microwave ranges[12]. plastic is used a lot because of the ease of manufacture and the low cost, as well as its ability to stick to the surface, but on the other hand, there are disadvantages, including When compared to many materials, such as sapphire, it has a low heat conductivity. poor thermal conductivity compared to other materials such as sapphire conductive and ceramics, and poor insulation despite the fact that the thermal expansion treatment is very large When choosing the focus material, you should pay attention to the properties of the beam, which will not lead to the isolation of electricity in general, which leads to a decrease in the beam from a microstrip antenna[13]

2.2.3 Feeding Structures

Feeding is important in antennas to improve beam performance and widen the width of the speaker. In this regard, the feed, has to be transferred radiofrequency or (microwave energy) by a system to the antennas smoothly and efficiently. by advancements in the design of antennas other than microstrip patch antennas[14]. Figure 2.4(a) The feed is connected by a tube extending from a coaxial line from the axis to the plane of the surface, this is a common method used to stimulate patching hobbies, most often the welding of the coaxial connectors is attached to the ground plane below the insulating substrate. (Coaxial) line and (radiating) patch impedance matching can be accomplished by changing the position of the feed point. Because of the large number of solder points and coaxial lines, this feeding configuration is inappropriate for arrays[15]. Other limitations include increased radiation, inductance and induction in antennas to form a broad substrate and surface waves. The antennas are designed with patch feed and circuits are added on the same board to save cost and reduce the design size as shown in Figure 2.4. It can be a transmission line or an RF communication link that harnesses the antennas to provide power to the feed strip[16]

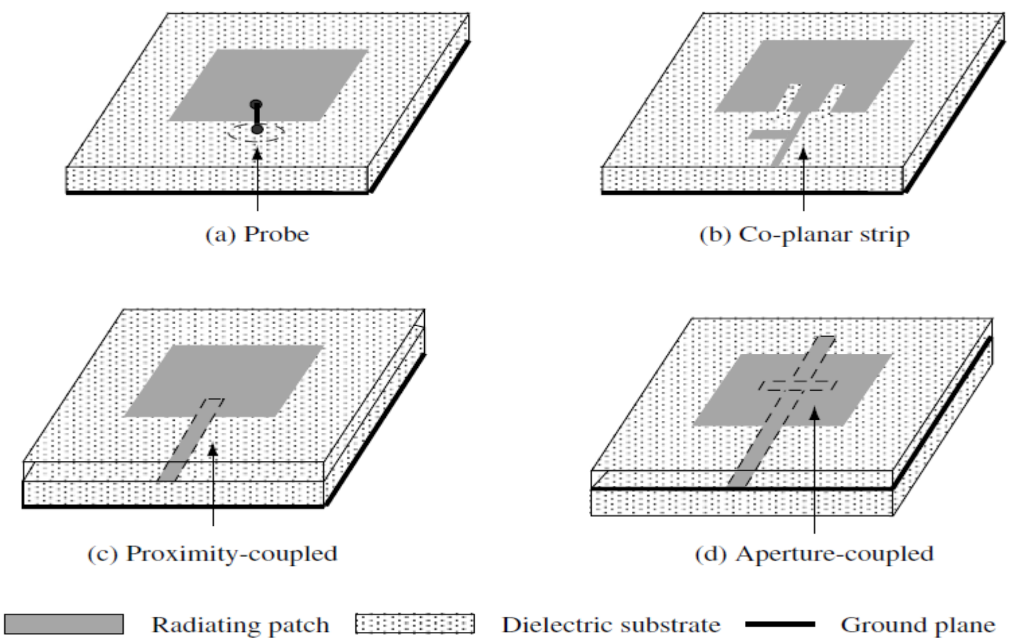

Figure 2.4: feeding of type

The feed tape can be attached directly to the antennas or needs to be patched using a coaxial line near the edge of the surface. This part of the design is very suitable for carpet applications, and this part of the design is very suitable for lining applications. For patching near the feed strip or inserting an impedance matching mesh, in the space, between the (strip) and the(patch) so as to provide a good match between the antennas and the feed[17]. As shown in the figure 2.4(c). It is located Between the feed strip below the antennas and above ground level, this will lead to

Isolation between the two layers, and this process causes a transfer of energy by lectromagnetic interaction between the antennas and the feed. On the other hand, this method is expensive to manufacture and increases surface wave losses[18]

Figure 2.4 shows that the structure associated with the hole is vital from the micro strip (d). A common ground plane separates two substrates; an upper substrate has a radiating patch, and a lower substrate contains a feeding strip. A no resonant aperture is cut from the ground plane, often a tiny gap Through the feeding hole, the process of attaching the patch with the feeding tape, and it is a process using electromagnetic to control the shape and composition of the patch in the contact between the tape and the patch. The resistance matching can be achieved by adjusting the feeding, and in most cases the antennas that are used feeding are a structure with a wide frequency resistance and good polarization, with the problem of manufacturing being complex and very high cost in single-layer designs[19]. There is another way to feed a co-planar waveguide (CPW). This technique is widely used as in microwave homogenized integrated circuits (MMICs) because it adapts well to the antenna design of patch tape feeding. The waves are cut at ground level and different slots are used at the ending of the CPW to, a match as in the figure 2.5[20]. Figure 2.5(a) Figure 2.5 (b) The coupling with CPW and the patch is stable and the coupling is stable. However, the hole on the Earth's surface generates powerful radiation, unlike the coupling of powers, where the ratio between them is 10 dB. Figure 2.5 A way to reduce unwanted radiation. The single mode that is stimulated in the aperture line is dominant in the CPW structure, and the currents adjacent to the aperture are unusual, so the radiation emitted from the feed is minimal. This method is ideal for applied matrices, as the background radiation and cross-coupling between the feed structures are well reduced[21].

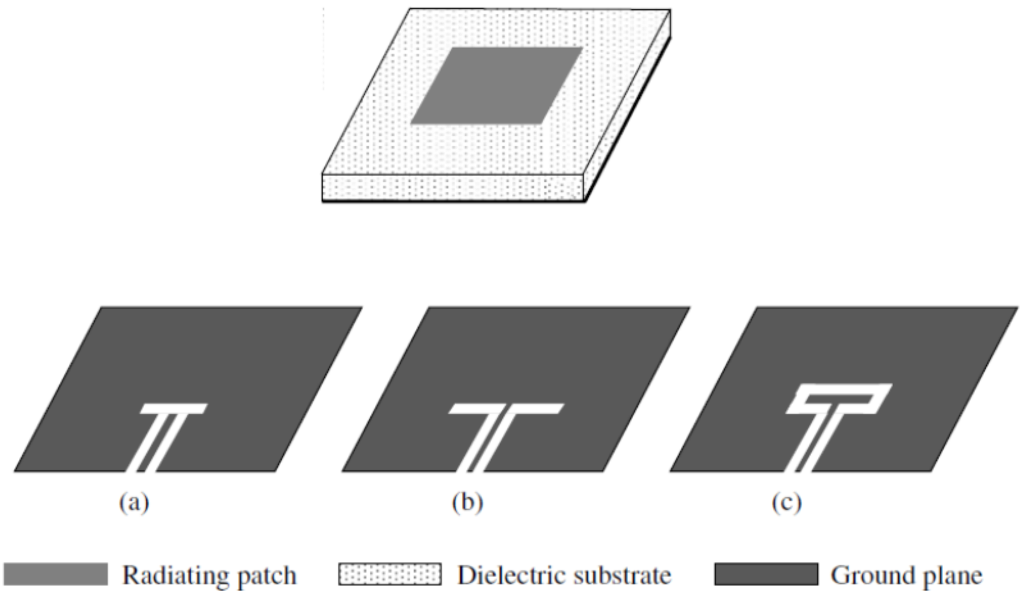

Figure 2.5: (CPW) feeding structures

2.3 BROADBAND TECHNIQUES

Table 2.1 Using the principles described, several broadband strategies have been created. The effect of the high on the antenna frequency is the shape of the geometry, as well as the radioactive and parasitic components, the way and the method of feeding, and this can be the large frequency of the microstrip patch antenna to a lower value and be well synchronized with many parts[22]. The process of decrease the, power about the antenna or growing the not profitable expands the width of the speaker. Similar to the existing one, an actual match can be obtained over the high frequency using the network modulus between the antenna and the feed. When two or more modes are activated, the frequency range can increase dramatically[23].

Table 2.1: Broadband techniques for microstrip patch antennas.

Approach	Techniques
Lower the *Q*	Select the radiator shape Thicken the substrate Lower the dielectric constant Increase the losses
Use impedance matching	Insert a matching network Add tuning elements Use slotting and notching patches
Introduce multiple resonances	Use parasitic (stacked or co-planar) elements Use slotting patches, insert impedance networks Use an aperture, proximity coupling

2.3.1 Lowering The (Q)

The patch tape antenna with a specific bandwidth is high because it is not used well and efficiently. As a result, the patch tape antenna can be considered as high efficiency and excellent quality. To solve the problem of narrow frequency in antennas, Q must be reduced[24].

Although the dimensions are the same, however, the radiator effectively affects the antenna range, the frequency width is very small and the geometry is very influential on the work, and this type of geometry is not used in practical designs. Low dielectric is a good choice in the thickness of the substrate to increase the bandwidth and impedance of the antennas and this kind of picks up the bandwidth very high and reduces the Q.[25]

The thickness of the focus is the important factor that must taken, into consideration in the design from order to reduce the losses caused by unwanted surface waves, thus reducing the radiating efficiency and stimulating the side rays, which leads to bad radiation, according to the research, the thickness of the frequency of the resistance is chosen monotonously and this will decrease the radiant efficiency dramatically high , however, the attainable bandwidth decreases. The lengthy probe in a probe-fed microstrip patch antenna causes significant input inductance and resistance around the resonance frequency impedance matching becomes more difficult as the input impedance rises[26].

2.3.2 An Impedance Matching

In patch antennas, the bandwidth is expanded, and this method can add an impedance network to provide good matching between a radiator with an impedance that depends greatly on the frequency and the feed, and most often two methods are used, the first option is to install a separate matching network of the beam modulation states, and the second option is to integrate the matching network With split radiator, in both cases the combination of the mesh can reduce the impedance lost and reduce the losses between the antennas and the feed structure to directly enhance the width of the spokes and this method is widely used in number in antenna applications[25].

The matching network can be divided with the feed strip on the same plane as shown in Figure (2.7) (a) and (b) The matching network, can have an (impedance) of a quarter-wavelength. or active or modulating components and this represents a good benefit to the radiation that does not need to change much Thus, the design becomes identical to the impedance and beam performance, to be modified separately. The main problem in this type is the increase in the size of the antenna, which makes the technology difficult to use in the arrays and also reduce the circuit efficiency of the system circuits and cause high radiation damages[22].

In Fig. 2.6(c), the formation of the external network is reduced, which affects the radiation and radiation performance, and this is a process that preserves the size of the antennas. The insertion into the patch can be a fine tape fed by the probe, supported by a thick insulating substrate. Figure 2.9 Wide circuits are formed with different probe and patches in order to compensate for the inductance process, and the capacitance is produced and adjusted to be synchronized with the input resistance through the radiation part and the circuits at the probe's end have a strong connection [27].

The patch consists of one or two slits and this leads to the creation of an internal frame on the patch and leads to insertion with an applied net, which affects the transfer of the impedance up at the edge of the radiation of the design to less than 50 features of the feeding structure.

The feed structures are either bar lines or sensors and this type of feed as in Figure 2.9 is the feed internal to match the wide band impedance[28].

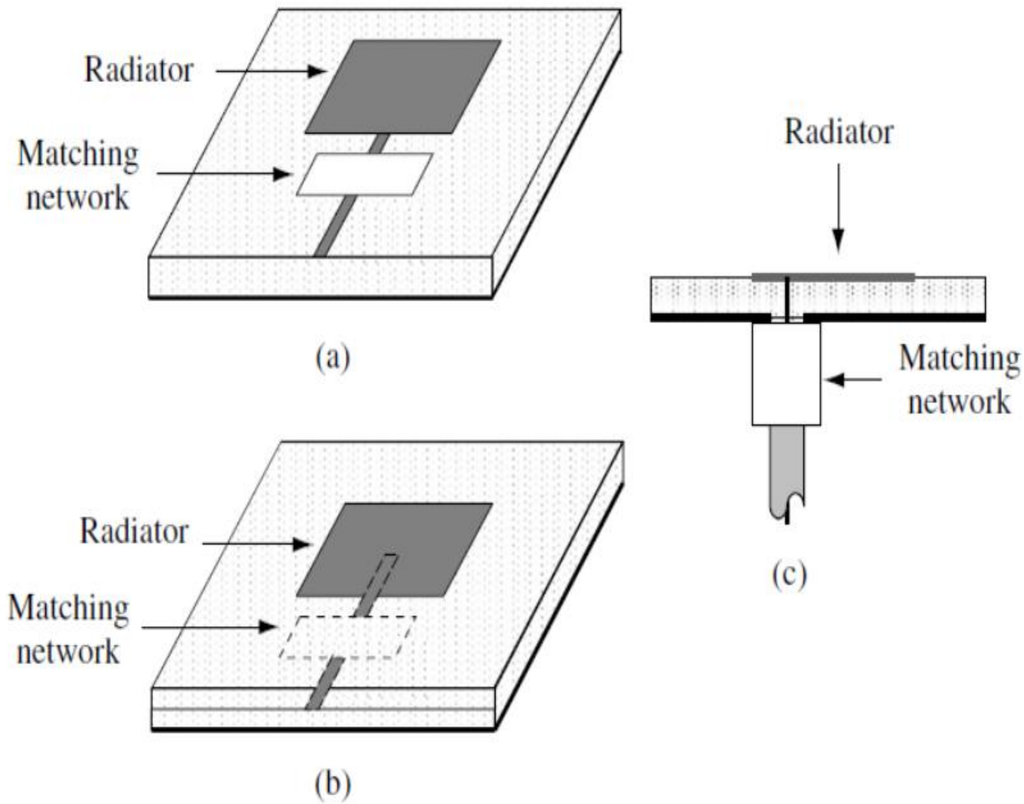

Figure 2.6: Theoretical Impedance Matching Networks.

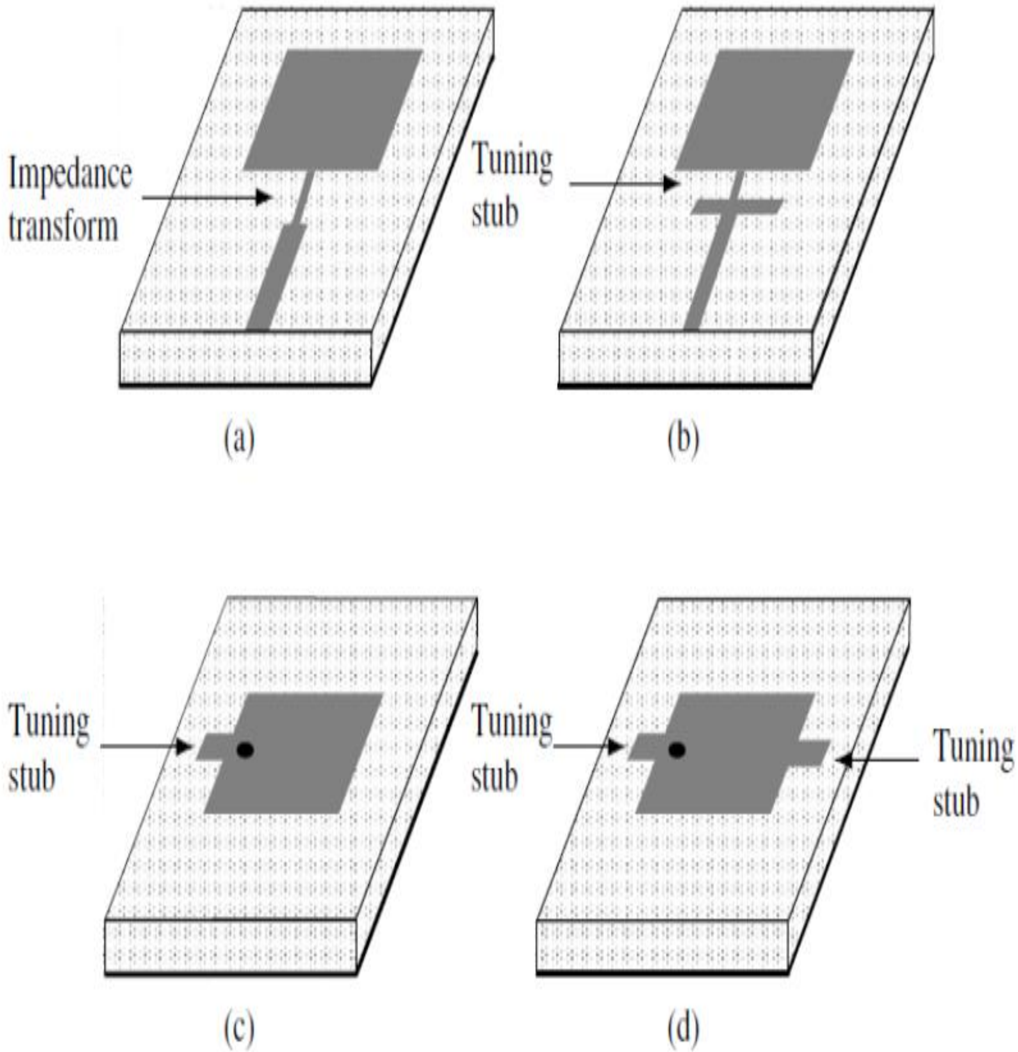

Figure 2.7: Matching Networks For Feeding Prob.

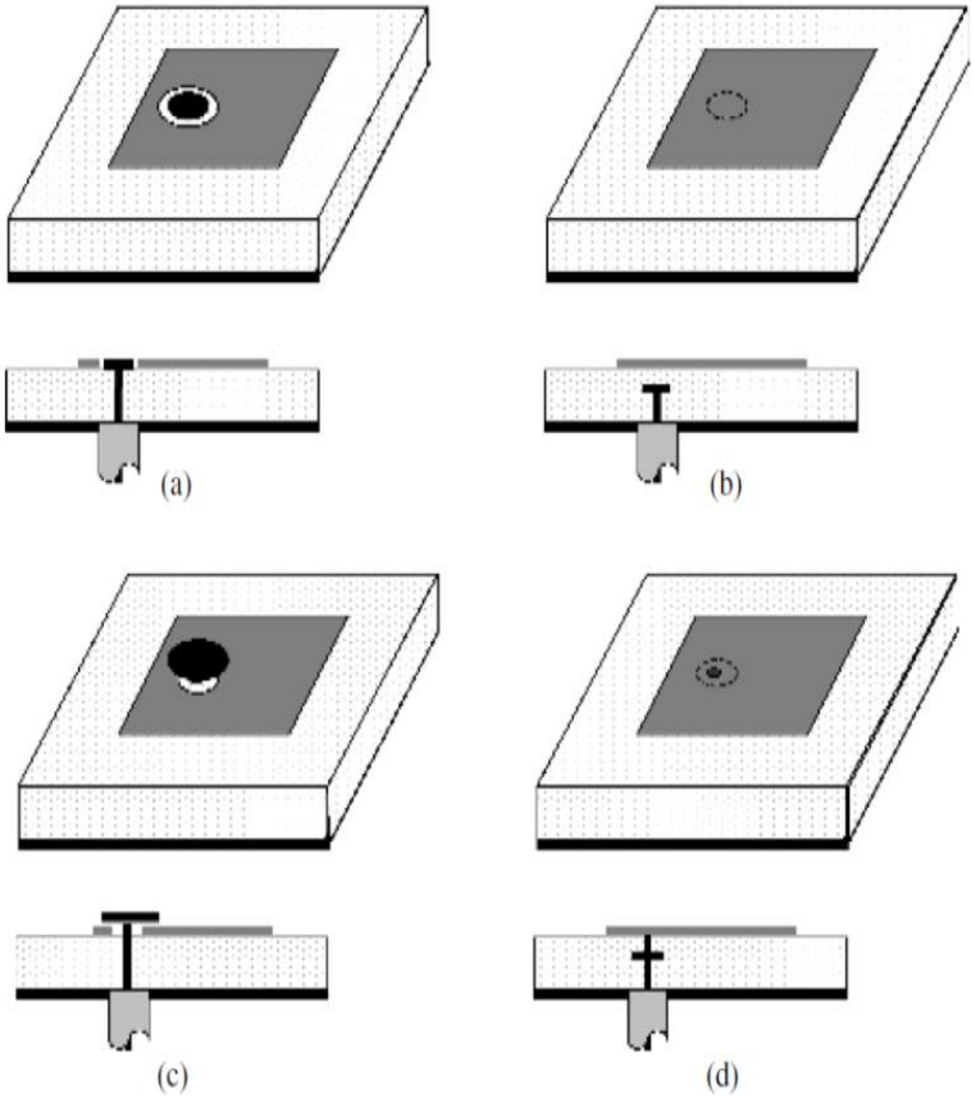

Figure 2.7: Matching Networks For Feeding Prob (continue)

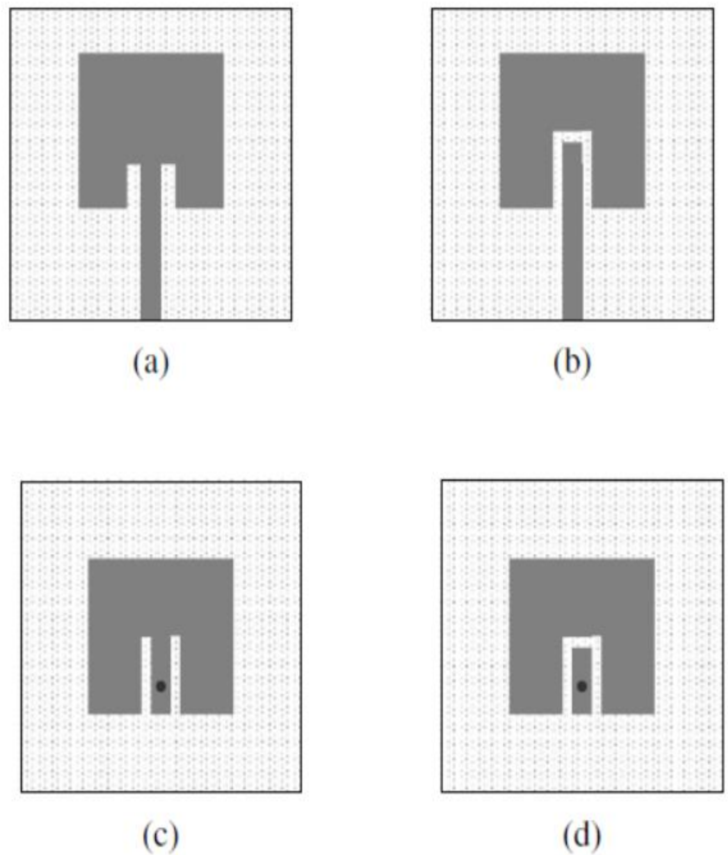

Figure 2.8: Matching Network With Slots And Snick.

2.3.3 Multiple Resonances

Microstrip patch antennas are essentially devices that operate at resonant frequencies with very restricted bandwidth. It has been demonstrated that operating at neighboring multiple resonances is a viable method of increasing bandwidth. This method effectively excites two or more neighboring resonances within the operational frequency range at the same time. This method has been widely utilized Serrated antennas with periodic register and second pole arrays Periodic dipole logarithms found in radio frequency circuits such as phased filters and various antenna applications[29].

The most straightforward method is to put extra radiating patches near the central radiator. The electromagnetic connection between these parasitic patches and the primary patch excites them. It can form on the same plane or above the patch are plastic stains.

Co-planar Arrangements

The bandwidth is highly compatible and is often larger than single-element antennas and is about the same size. Figure 2.10 shows the common level configurations where one or more plastics are placed inside the antennas to form small gaps for the antenna components to be connected to each other.

The plastic components are along the non-radiating edges in formations) a (and) b (. Calculates sensor lines, inductance lines, and CPW radiation levels by increasing the H polarization, and even the bipolarized E radiation. This can be a method for selecting the feed structure, and it does not operate at high frequencies and is one of the disadvantages of this method[30].

The parasitic components in configurations (c)–(e) are linked to the main patch along Such designs show an unchanged radial at high frequencies and the (impedance) (bandwidth) can be multiplied by five that of the individual rays while the E electrodes work highly and efficiently but the H polarizations are distorted[31].

The arrangement (f) combines the two techniques mentioned above to increase bandwidth even further. This technique has the potential to nearly quadruple the bandwidth attained by the other systems. Furthermore, by appropriately placing the components close to the main patch, as illustrated in Figure 2.10, this design may be used to produce circularly polarized functioning (g). The major disadvantage of such a configuration is the substantial increase in lateral dimensions.

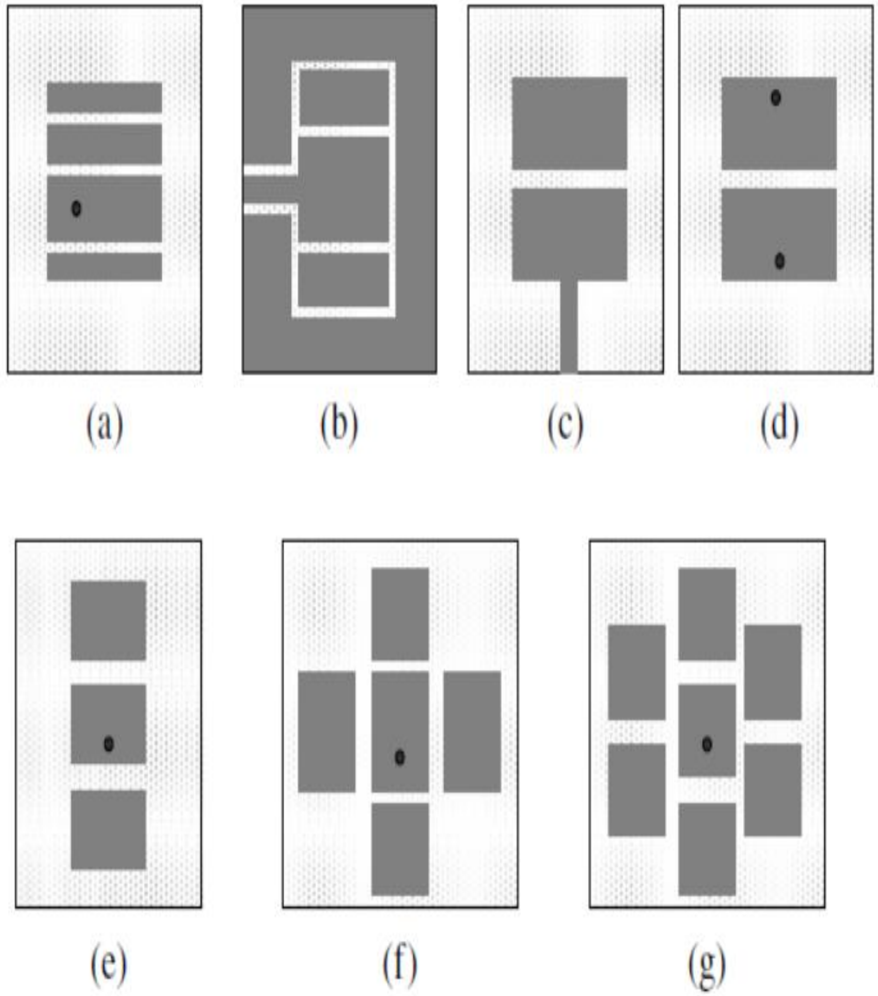

Figure 2.9: CO-PLANAR COUPLING SCHEMES.

Stacked Arrangements

Figure 2.11 depicts configurations in which parasitic components are positioned above the main patch (es). The impedance bandwidth can be substantially extended by connection between parts that are stacked and the driving element. Typically, with the middle between tow part (upper) and (lower) points is free space or low permeability material VSWR = 1.5, and the bandwidth is from 10-20%.[32]

Configurations (A) - (C) that make up the antennas are simple and small in size, and this lower segment is generally smaller than the main shale element to provide a direct probe or a straight line, and the bandwidth is in a band between 10-20% so that more than two components are stacked above The lower part is to improve the antenna gain, as indicated in Configuration (D). This method gives a gain of 8-7 dB for a linear extrapolation of 8-6 dBm.

A new method of feeding as in Figure 2.11 (d), where the bottom board is joined with a straight line below ground level through a hole in the board, and this method gives a frequency width of more than (10%) and, perfect radial performance because of its perfect configuration, but there is a disadvantage is the presence of a back beam unwanted.

This in Figures 2.11(e) and 2.11(f) combines the common-level architecture and the low-bandwidth chassis with a wide bandwidth with high gain. This makes the array design good. However, the use of widely variable variants with communication systems makes for a great array and strong beam performance high gain[33]

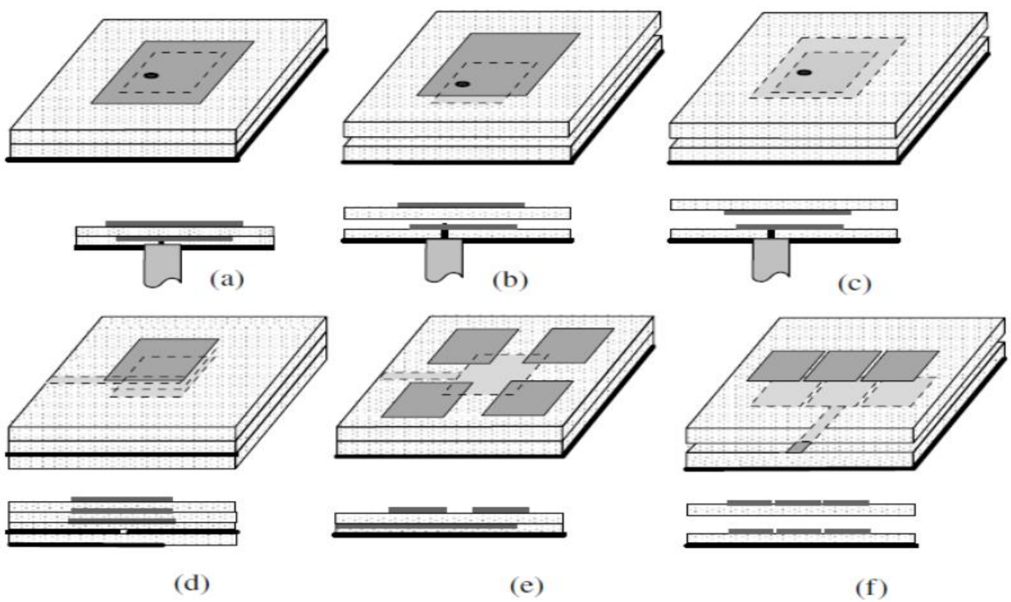

Figure 2.10: Coupling Schemes

2.4 NUMERICAL TECHNIQUES (FULL WAVE MODEL)

Some sophisticated numerical approaches have been proposed and employed for the analysis of irregular-shaped structures. Analysing Maxwell's equations can only provide Geometries that are simple. There are, numerous of them. 3D entire wave commercial (software packages) that provide exceptional performance and understanding of 3D-EM issues. In this thesis, two different commercial software packages: Microwave Studio with Computer, Simulation Technology, (CST MWS) and High Frequency, Structure Simulator (HFSS) with its basis in the Finite Integral Technique (FIT) and FEM stands for Finite, Elements Model. are employed to optimise the antenna's dimensions and assess their effectiveness with regard to radiation patterns, scattering parameters and dispersion diagram.

a. CST MWS Software Package

CST MWS is full,featured electromagnetic (EM) software suite for high-frequency analysis and design. CST MWS, has a number of varying solvers based on FIT, that are suitable for a variety of applications. No single approach is ideal, for all applications. so approaches such as transient solvers, frequency domain solvers, integral equation solvers, and Eigen mode solvers may be required to best suit specific applications. [49]-[50].

The transient solution provides the most (flexibility) in terms of obtaining whole broadband frequency action,for the simulated device with only one, calculation run. CST MWS also includes a variety of adaptive criteria that help obtain high accuracy outcomes, for example mesh adaptation technique based on growing the rate of lines per wavelength and lower mesh boundary settings, as shown. in Figure 2.12.

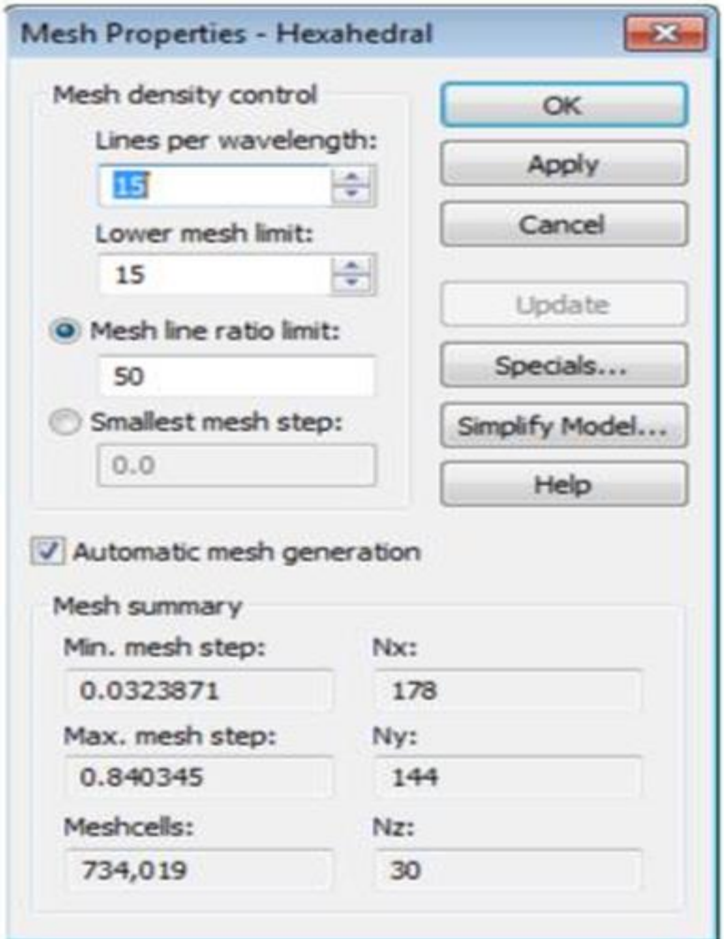

Figure 2.11: The mesh characteristics are shown through a graphical user interface (GUI).

Furthermore, because a computer, can calculate issues with limited expansion, CST MWS gives boundary conditions. As a result, applying boundary conditions, is a difficult process. OPEN Convolution adds space in all directions. In Figures 2.13 and 2.14, the Perfect Matched Layer (PML) formulation is used, which provides a material, independent absorbing boundary condition with four layers, and a reflection, coefficient factor of 0.0001.

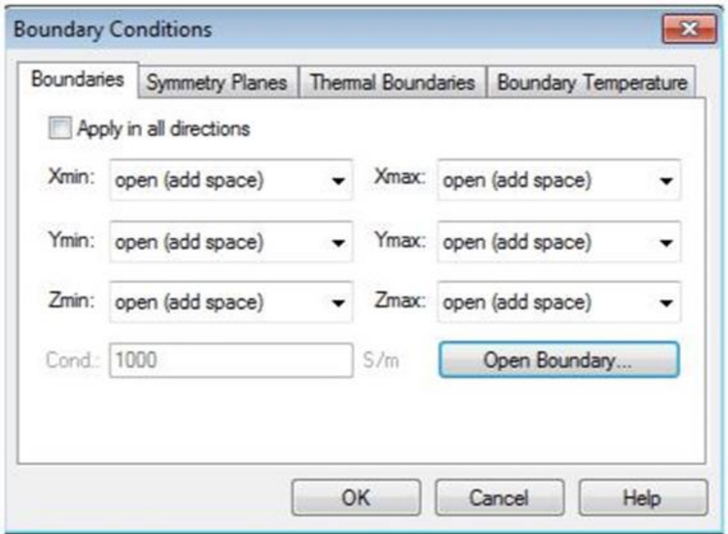

Figure 2.12: A Boundary Stipulations Are Displayed Via A Graphical User Interface

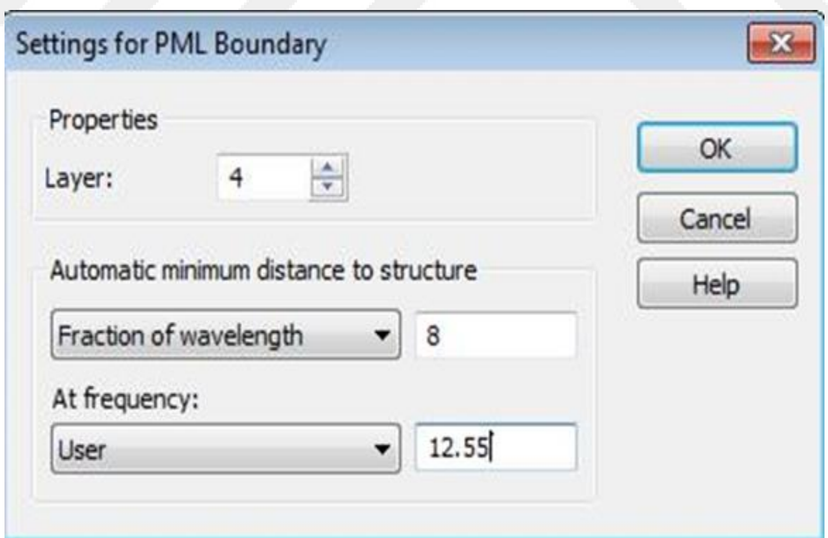

Figure 2.13: A PML boundary tuning are shown via a graphical user interface.

When S11 (f), the maximum relative, fails to change beyond 0.1 during at least two consecutive runs across the frequency, range of interest, the simulation, is ended. Change from the old mesh to the current,mesh in |S11|. When the energy within, the structure reduces by -50 dB below its greatest value, as shown in Figures 2.15 and 2.16, the test is over.

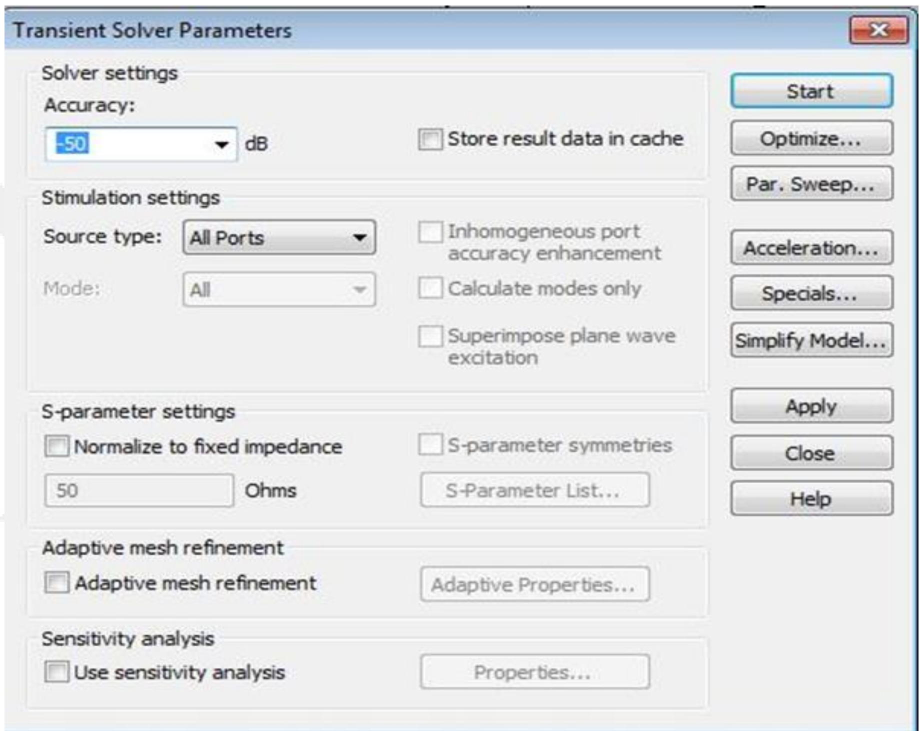

Figure 2.14: GUI showing the transient solver parameters.

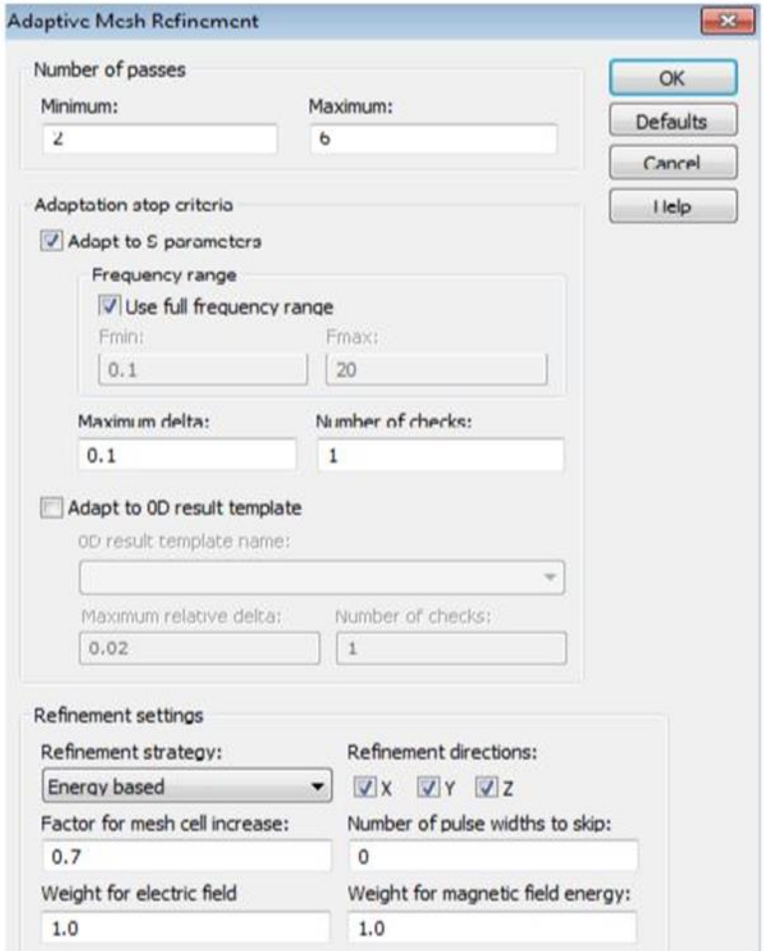

Figure 2.15: GUI showing the adaptive mesh refinement.

b. Package containing software (HFSS)

HFSS is a full-wave EM field simulator with a high level of performance. provides many find technologies using FEM. Each solver is unique. combines a robust, procedure for automated solution, stipulating the requirement of only material characteristics, geometry and a expected output. After that, HFSS takes over. creates a suitable, efficient and precise mesh to address the issue of employing the chosen solution technology. HFSS has its basis in FEM, so a geometrical model with arbitrary shapes is inevitably separated into several meshes [51]-[52]. Building models can be created by way of numerous characteristics that are drawn interact with fundamental geometries by using the library of materials, assign a preferred material to a given model, component. Numerous boundary conditions including (PMC) , (PEC) may could be chosen and also the voltage supply or a port for exciting the structure. Boundary conditions and port position are integral to HFSS's border simplification Mesh refinement that adapts occurs by stipulating a number, of passes besides a criteria of convergence. The simulation of antenna outcomes are inclusive of the far field plots, Smith Chart graphics, and S-parameter data list be able to presented following a performance, of the simulation as demonstrated in Figure 2.17.

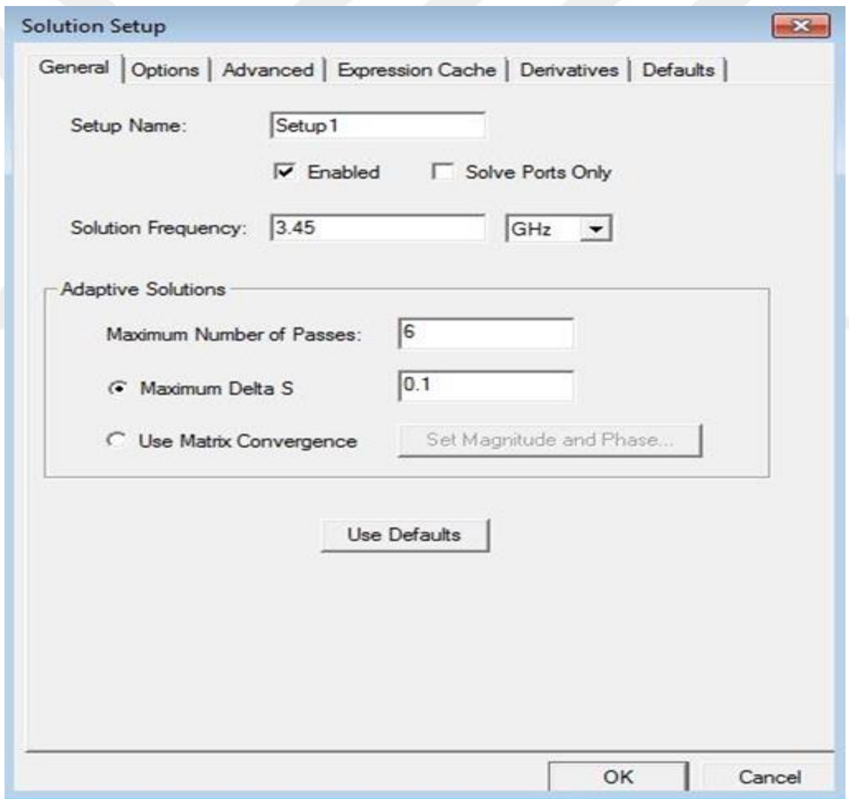

Figure 2.16: GUI showing the solution setup.

The fast sweep option is utilised with a step in frequency, that is linear that starts frequency range 0.1 GHz up to 20 GHz with a the width of the step of 0.1 GHz as presented in Figure 2.18.

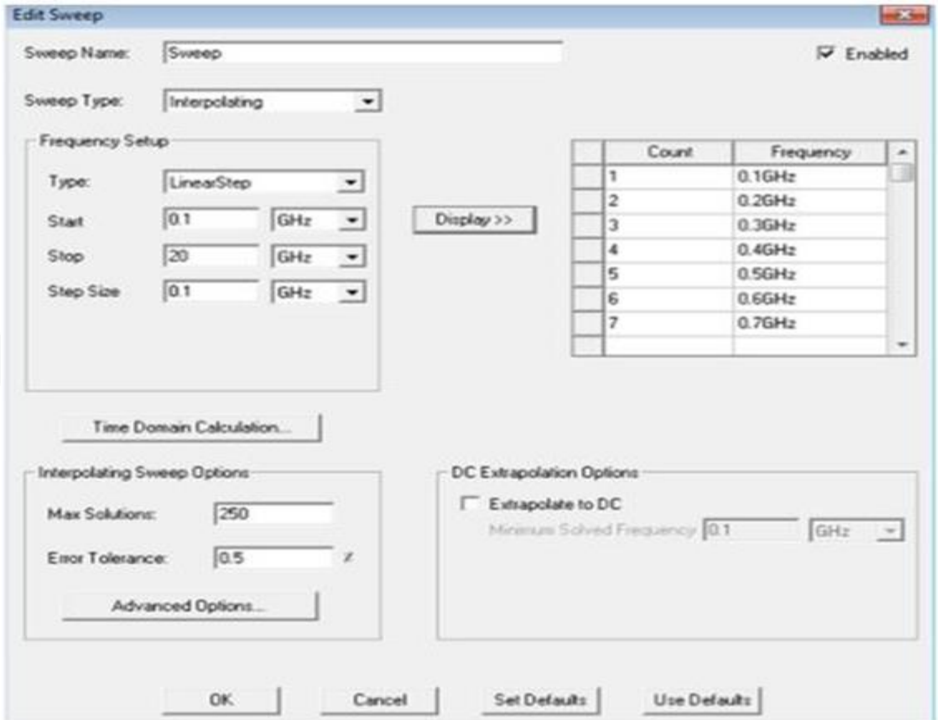

Figure 2.17: GUI showing the edit sweep.

In Figures 2.19 and 2.20, the mesh of the square patch antenna is generated by (CST MWS) (HFSS,) respectively, and the finest mesh producing the converged solution is shownThe fine

mesh densities shown are essential a achieve know precise field and current distribution of theprinted circuit line's narrowest sections

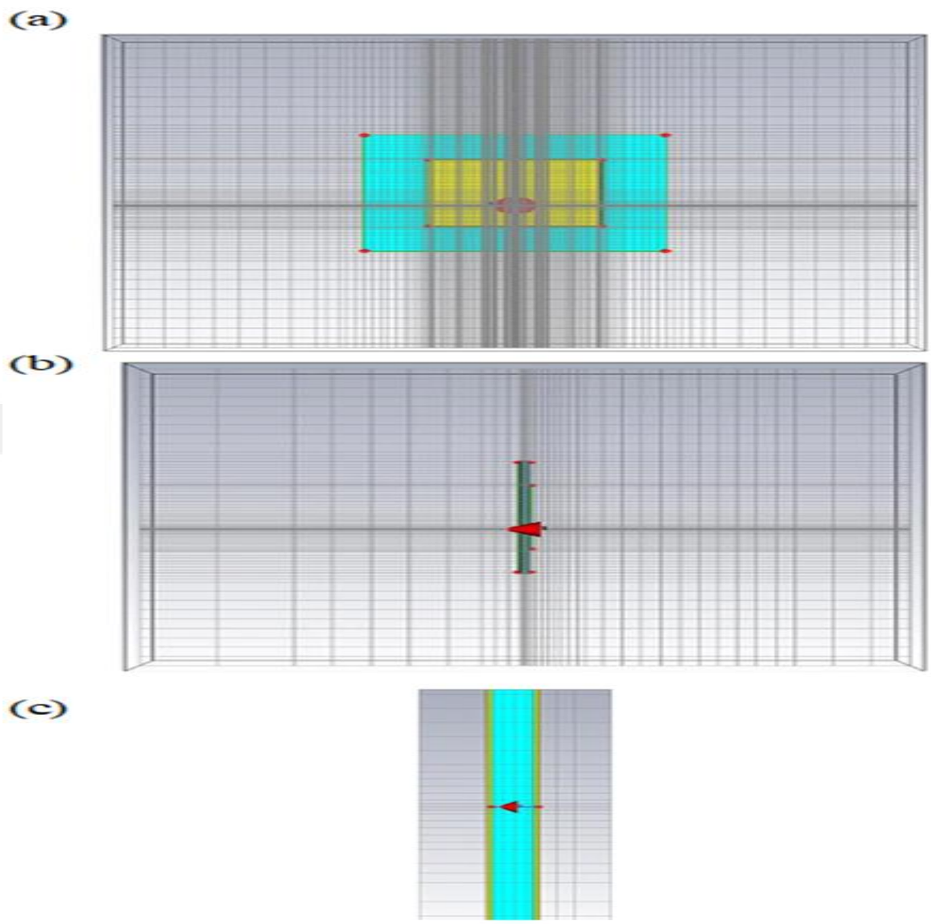

Figure 2.18: The mesh distribution from CST MWS; (a) front view, (b) and (c) side views.

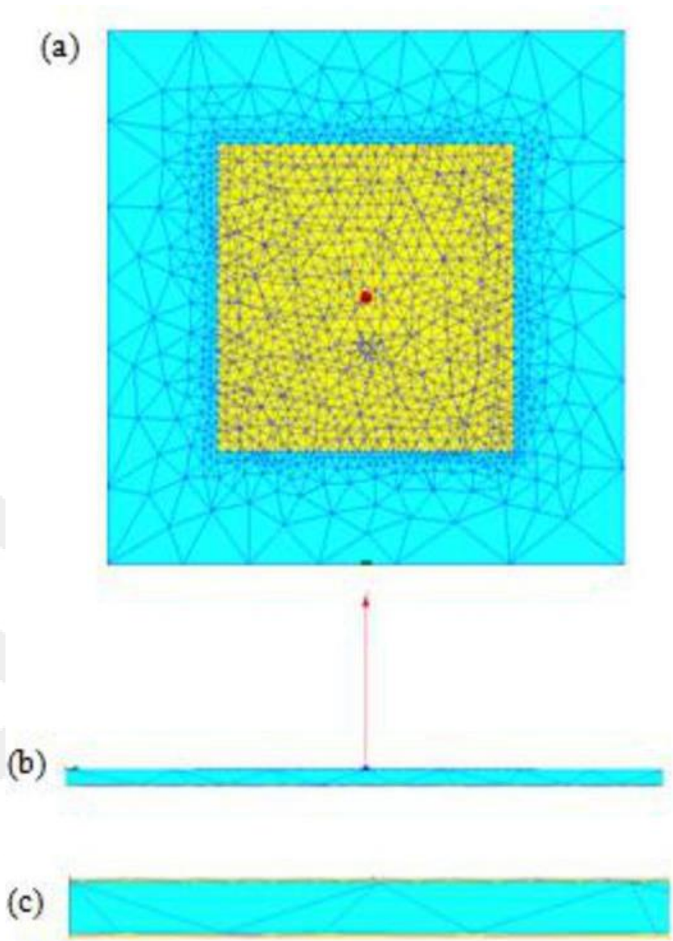

Figure 2.19: The mesh distribution from HFSS; (a) front view, (b) and (c) side views.

3. ANTENNA DESIGN AND METHODOLOGY

Substantial developments are conducted to the antenna design techniques were observed rabidly to improve their (gain) (bandwidth) goods performance [1] L-prop feed, for example, created a microstrip printed antenna with a (bandwidth) of 36% and an medium gain of about 7 dBi in [2.] (Vivaldi antenna) was formed,with a frequency range between 3.1 up to 10.6 GHz and (gain)of almost 6 dBi. [3].

In [4] almost-Yagi antenna with a superior (gain) of 8.6 dBi operating from [7.32 GHz] to [11.15 GHz] was proposed. Wong et al. [4] created integral antenna by stimulating both dipoles; the fabricated antenna demonstrated dependable gain stability and minimal back radiation across a wide frequency.. like coil loop, magnetic dipole, the resonators of the (H-shap), and the loop used for the (dipole), composites were constructed from various (Vivaldi antennas) in [5-7]. On the other side, these antennas have a low and irregular gain. As a result of their distinct electromagnetic characteristics, metamaterial structures are increasingly being used in antenna designs [8],

Lower or zero refractive indexes, for example, are used to regulate antenna radiation [9]. The gain of a microstrip antenna using zero refractive index of the metamaterials which used in the isolated material was enhanced by (1 dB) to (2 dB), according to Zhuet al. [10]. These types of inclusions, on the other hand, may cause the antenna, to grow in size of antenna A, fabrecated (Vivaldi antenna) instituted on dipoles is suggested in this study, based on, the antenna body [6] with many changes to improve the performance of antenna. To achieve broad bandwidth impedance, a microstrip to coplanar striplina transition balun is substituted with a microstrip (which can be described as a symmetrical) to the stripline transition balun. To boost the antenna gain, used HSR array. To further boost gain of antenna, a fabrected (Vivaldi antenna) utilized instead of the Vivaldi. After tha Antenna Design

3.1 DESIGN ANTENNA

The suggested antenna construction is placed on a 1.6 mm thick FR4 substrate with r=4.6 and tan=0.0004 and r=4.6. As illustrated in Fig. 1, the isolated material layer is intended to be implanted in line with the antenna sections.. 1. Electric dipoles with (Vivaldi), magnetic half-loop dipole, microstrip-to-stripline transition baluns, and HSR inclusions are four basic components of the antenna. The magnetic part shape is based on design of antenna published and the design H-shape is based on the antenna design presented in [6]. [11]. An SMA connection is used to power the antenna, which is then attached to the balon. The inner section of the SMA is linked between to part (strip line and SMA) [12] to fulfill broadband impedance matching show in (F.1)

As seen in the (Fig.1) the Vivaldi grating, is made up of three parts that are coupled to the magnetic part. The Huygens source [13] is achieved when the dipoles are stimulated a in the same way extent and phase, resulting in a broad leaking of the band. [14]. As a result, interference, amidst the magnetic dipole's /10 length radiation fringing and electrical part more than one length radiation fringing can produce unidirectional, radiation patterns [15]. Furthermore, The difference between the dipoles is changed to obtain a

(90°)phase variation, which results in the TEM mode.

[16The brink grating OF THE Vivaldi, on the other hand, may cause dispersion in the produced beam, lowering the antenna gain [17]. As a result, the HSR array used to increase antenna radiation, efficiency [15].

It's worth noting that HSR technology has already been published in publications such as [15], but the primary novelty in this study is to improve matching the suggested antenna as well as the circuit rectifier

The real component of a relative matching, impedance in the fundamental antenna construction of a proposed work exhibits a large variance, which decreases the matching between the suggested (antenna) as well as the circuit rectifier. As a result, as will be seen later, the introduction of the suggested HSR had a favorable impact on the convenient impedance amongst proposed design structure and the (RF harvesting board). Furthermore, the suggested HSR geometry is used fabrected design and improve radiation efficiency, which raises antenna gain and improves electromagnetic rectification, efficiency, i.e. boosts harvested voltage. The improvement can be observed efficiency with impedance spectra after adding the HSR structures

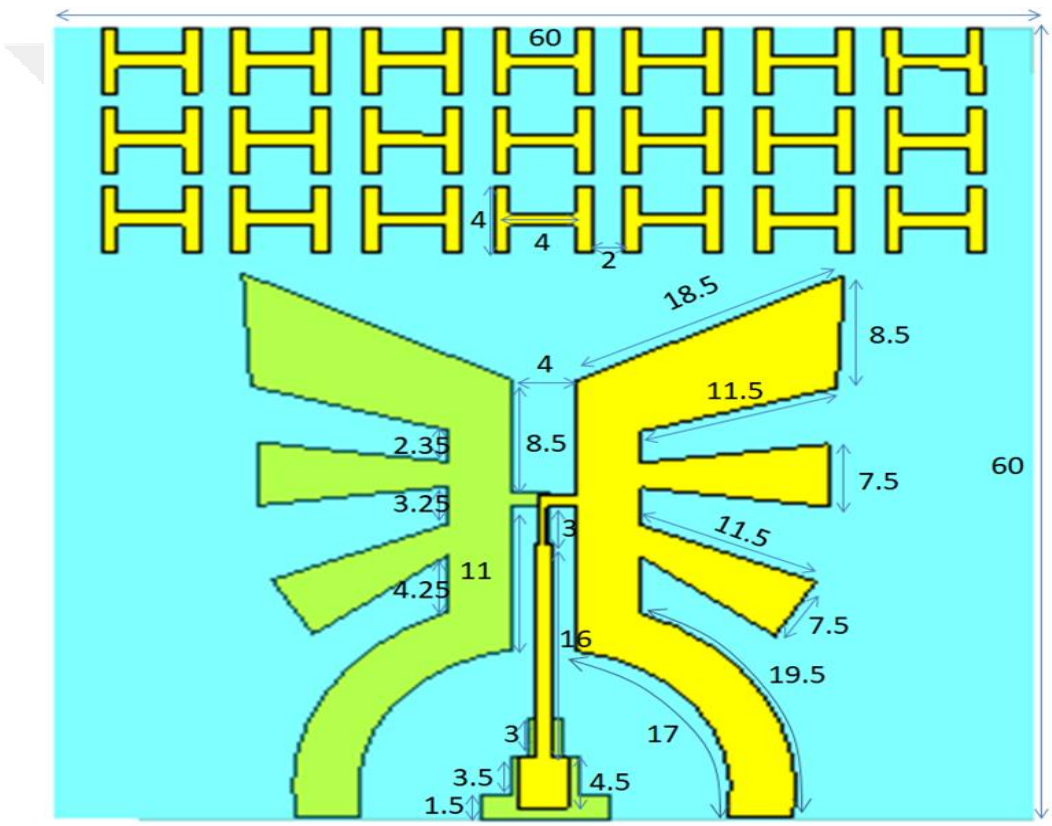

Figure 3.1: Arrangement Of The Suggested Design Antenna.

3.2 METHODOLOGY FOR DESIGNS

3.2.1 Antenna Performance In The Absence Of Hsr

This section looks at antenna performance numerically before moving on to HSR in terms of S11 and Wi-Fi band radiation patterns at 2.45 GHz and 5.8 GHz. Finite Integral Technique (FIT) based on CST MWS formulation [18] is used to accomplish the numerical analysis. The S11 spectrum in Fig. 2(a) demonstrates that a antenna has a wideband without H- shape modulation, but in Fig. 2(b), the antenna gain has clearly deteriorated owing to superficies wave leakage.

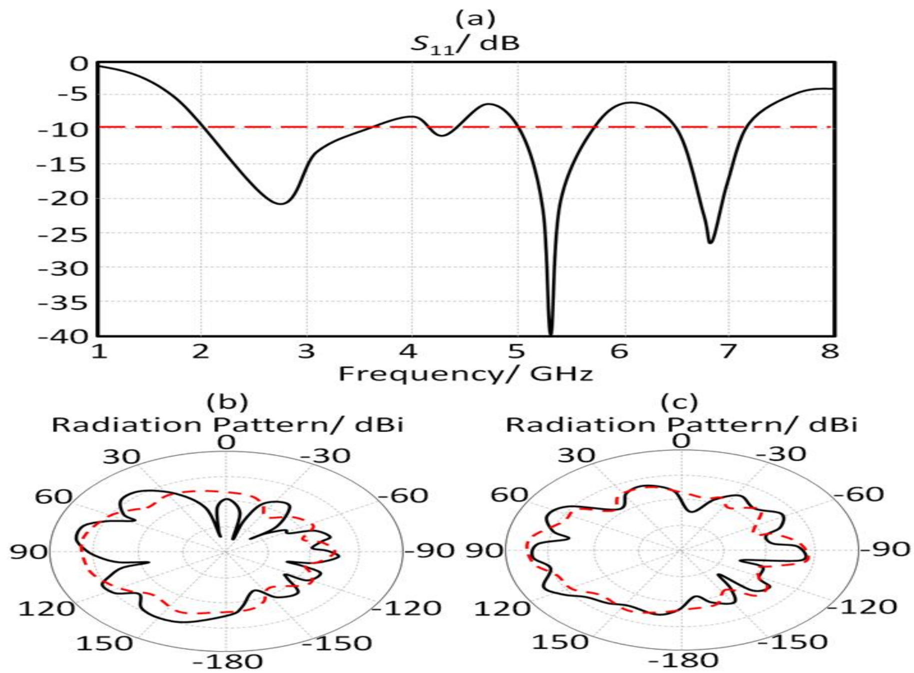

Figure 3.2: Simulated antenna results without (H shape) inclusions S parameter spectrum, and previously published radiation patterns at tow frequency (2.45, 5.8 GHz)

3.3 HSR DESIGN

The relative refractive index of the proposed HSR unit cell is determined using the simulated S-parameters. The retrieval procedure is carried out utilizing the robust approach described in [16]-

[18]. To analyze the (S-parameters), a unit cell centered inside of the factious waveguide (see Fig. 3). As a result, a perfect electric jointer over the x-axis and exemplary , magnetic jointer , over the z-axis are given as boundary, conditions

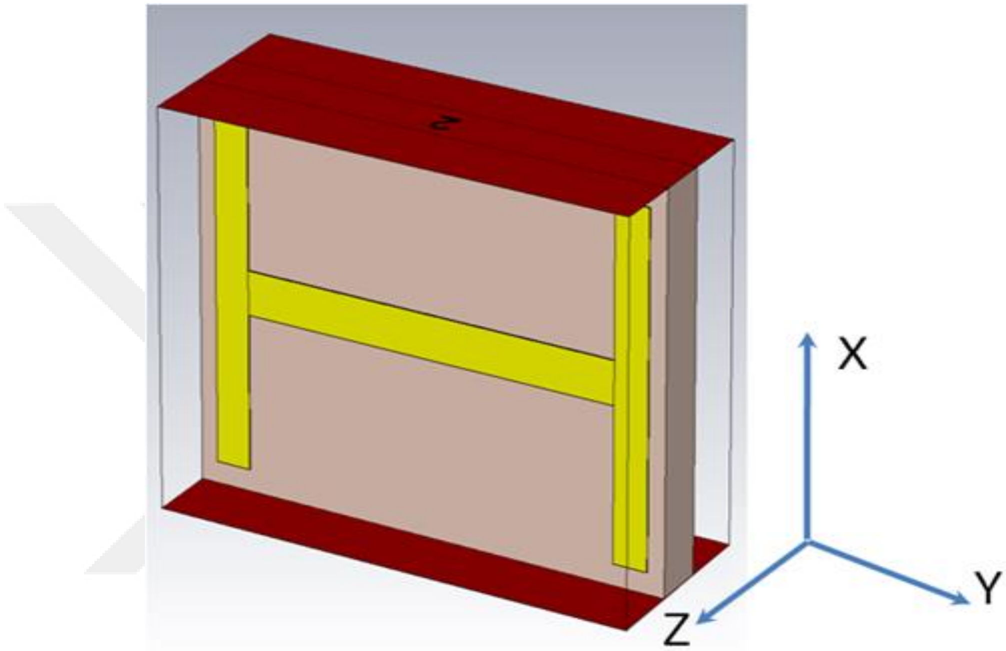

Figure 3.3: HSR unit cell inside the factious waveguide

The suggested HSR is discovered to offer a (refractive index) (n) that varies between 0 and 3. As a result, such a unit cell may be used to focus the radiation, pattern in the endfire direction on the antenna construction

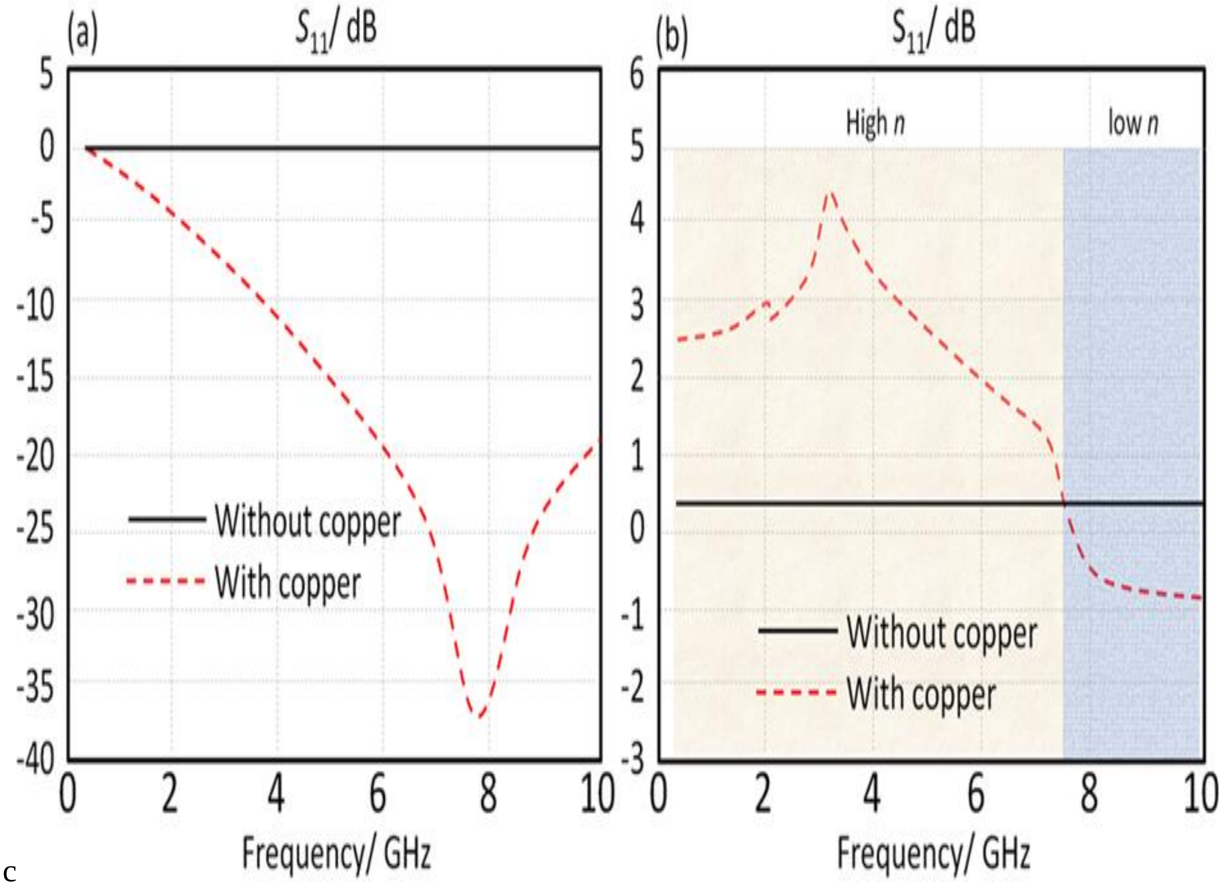

c

Figure 3.4: Characterizations of the HSR unite cell: (a) S11 and (b) retrieved refractive index.

3.3.1 (HSR) Inclusions Depending On Antenna Performance

Snell's law states that, nisini=ntsint, where I denotes a incident wave, and (t) denotes this transmitted wave, with a diffracted angle (t) becomes big at minimal reflecting index of a HSR layer (t) whenever a refractive index level of isolated material layer (ni) gets large enough. As a result, the energy collects beam focussing, resulting in a large gain in that direction. To concentrate the till the end-fire irradiation, the HSR layer offers a a isolated material with a greater n n. This layer is made three in seven lines of HSR unit cells, that will be installed, on the substrate's top side. Figure 5 shows the efficiency of the antenna, using H-shape inclusions and S11 spectrum.

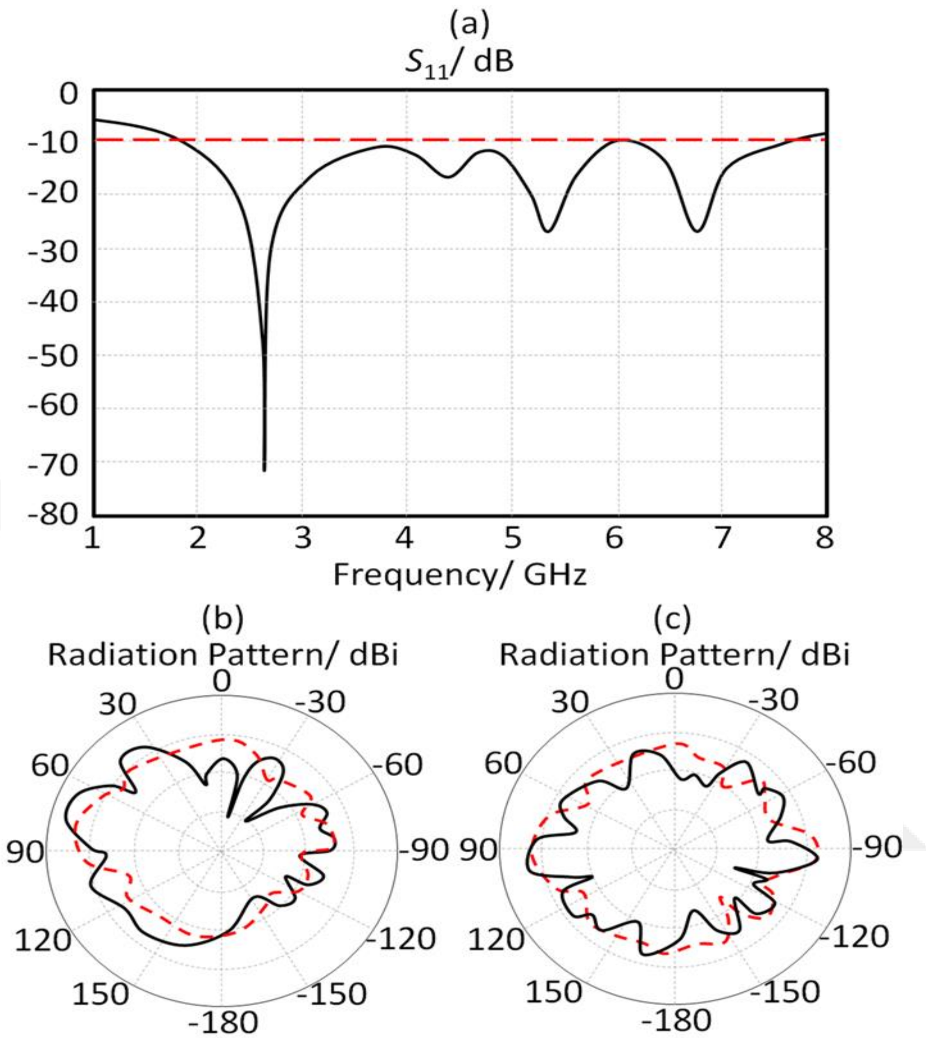

Figure 3.5: HSR design simulation results: S parameter and Radiation patterns in the (2.45 ,8.5 GHz), respectively. The (CSTMWS) has a red line for a YX plane and a black line for the YZ plane.

3.3.2 EBG Characterizations

The performance of the suggested EBG structure is evaluated both analytically and quantitatively for this section. Characterizing the expansion constant, reflection phase, as well as dispersion spectra is used to, analyze a , constitutive electromagnetic parameters. As shown in Figure 3, the suggested EBG is made up of a 56 square metal pad array installed on the rear panel of a substrate, which results in 45 slots. Its periodical dimensions of each EBG cell are (p) of 3.6mm3.6mm and (g) of 0.4 mm.

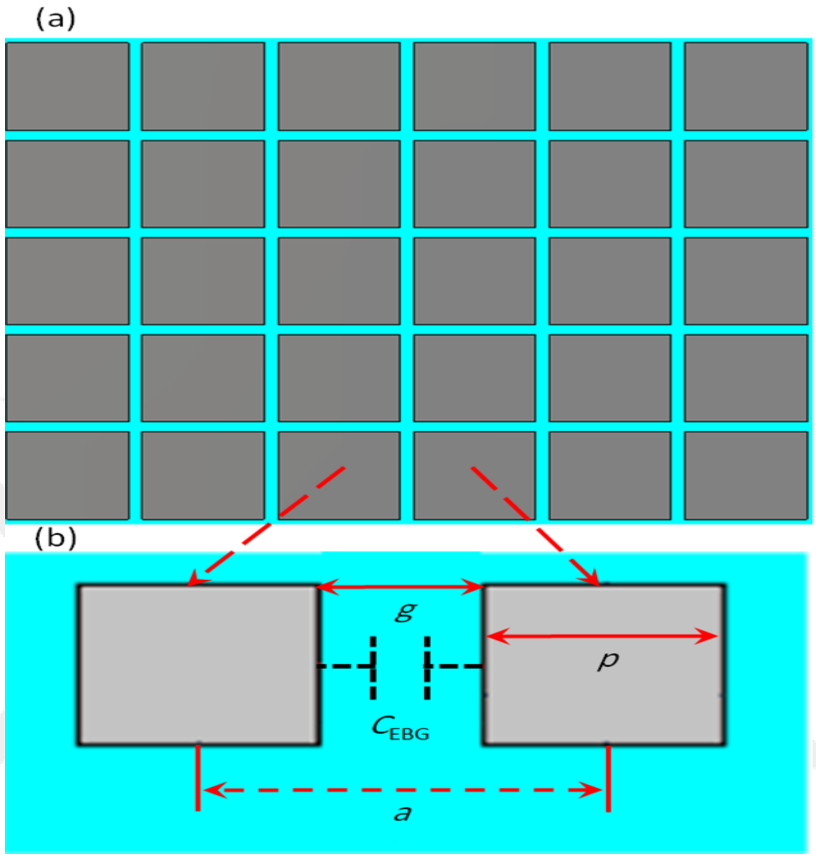

Figure 3.6: The proposed EBG structure: (a) EBG array and (b) equivalent capacitor.

Now, such array may create a capacitive behavior (CEBG) determined by [16]

$$C_{EBG} = \frac{p\varepsilon_0 (1 + \varepsilon_r)}{\pi} \cosh^{-1}\left(\frac{p + g}{g}\right)4 \qquad (3.1)$$

As a result, the ascribed behavior is characterized by a high pass filter [22]. Nonetheless, due to the lack of an inductive component, such an array produces an imbalanced circuit, indicating a considerable effect on surface current velocity along the EBG width in compared to the EBG length. [23].

A EBG achievement is primarily influenced by the number of slots (mn); mn is required to provide strong capacitive reactance over the antenna width in order to suppress surface waves [9]. The dispersion technical drawing and reflection phase spectra by using CSTMWS and ADS software programs are used to verify this idea. The band-gap, normal resonances, and dispersal parameters for the proposition EBG are all localized in the, simulation. The publishing constant () for the proposed unit cell is, determined at the First Brillion, Zone (FBZ) in the crystal lattice (M) vertex in these calculations for (TE) and (TM modes [17]. In the absence of the inductance component, the propagation constant may be computed as:

$$\gamma = \sqrt{(R(G + j\omega C\_EBG))} = \alpha + j\beta 5 \tag{3.2}$$

$$R \approx 8.686/2\pi \ \sqrt{(\pi f \mu \ / \ \sigma)}/50h \times [1-(p/4h)^{\wedge}2\ ] \times [1+p/h+p/h\ (ln\ 2h/ t-t/h)]6 \tag{3.3}$$

$$G \approx 8.68\pi\ ([(\varepsilon\_r+1)/2+(\varepsilon\_r-1)/2\ (1+12h/p)^{\wedge}(-0.5)\ ] - 1)/(\varepsilon\_r-1) \times \varepsilon\_r/[(\varepsilon\_r+1)/2+(\varepsilon\_r-1)/2\ (1+12h/p)^{\wedge}(-0.5)\ ] \times tan\delta/\lambda\_g\ 7 \tag{3.4}$$

where, μ is permeability, σ is conductivity, t conductor thickness, and λg is the guide wavelength.

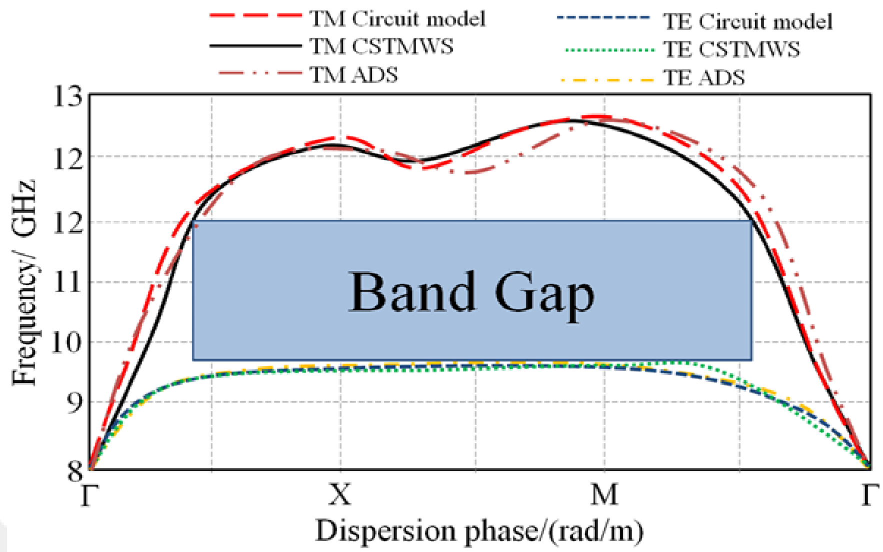

Figure 3.7: Dispersion diagram.

Figure 4 shows the resultant dispersion diagram, which shows that propagation between (8 and 12 GHz) is forbidden. The acquired results are mathematically justified using equations (9). however the ADS simulation is used to define the reflection phase properties of the EBG shape , and the findings are compared to the (CSTMWS) results. The analytical solution is used to verify the given findings using the equations below:

$$Z\_EBG = \surd(R/(G + j\omega C\_EBG))8 \tag{3.5}$$

$$\Gamma = (Z\_EBG - Z\_0)/(Z\_EBG + Z\_0\ )9 \tag{3.6}$$

where, ZEBG is the EBG characteristics impedance and Γ is the reflection coefficient.

The unit cell exhibits reflection phase conduct from (8 GHz to 12 GHz) , according to the circuit model of the ADS simulation illustrated in Figure 5(a), as sub networks inside a single design. The electromagnetic characteristics of the proposed unit cell in terms of r and r are next assessed and shown in Figure 5(b) (with) and, (without) substrate. Due to the change in guided wave length, the inclusion of the substrate layer has a considerable influence on the recovered r and r [

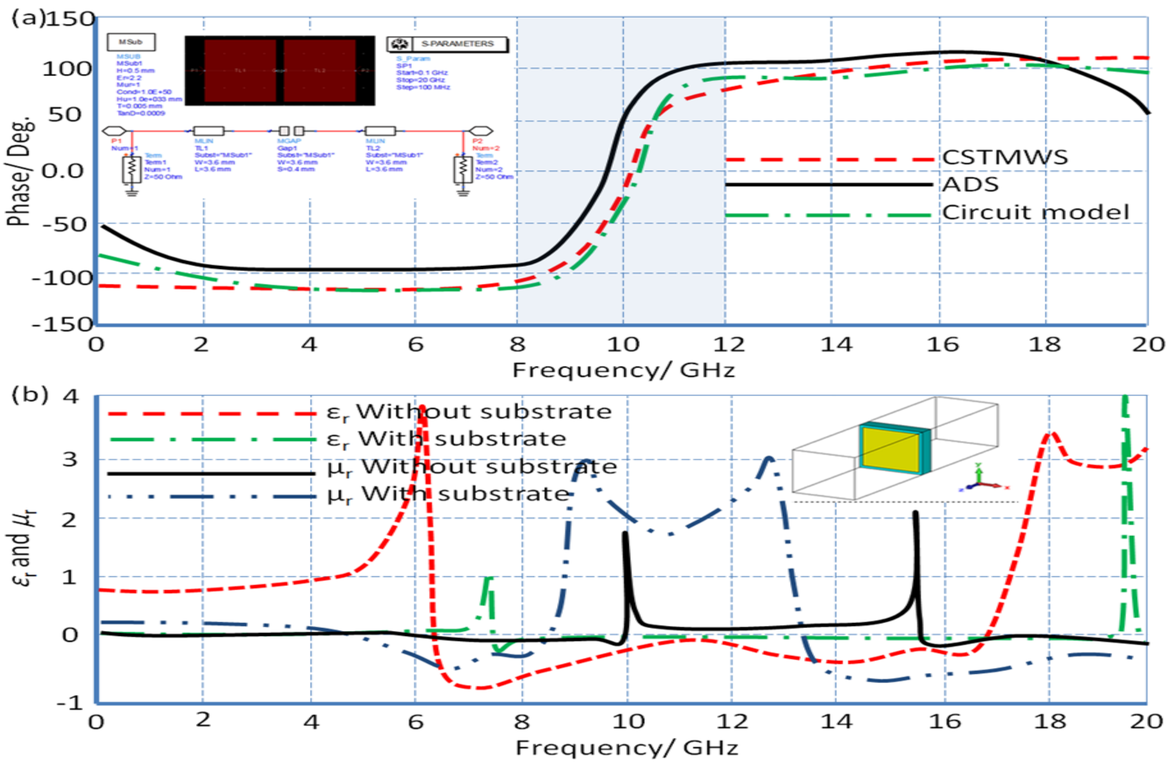

Figure 3.8: The unit cell characteristics including; (a) Reflection phase and (b) Relative electromagnetic properties.

The authors used an analytical analysis to optimize EBG dimensions with relation to various commercial isolated material to understand the impacts of EBG unit cell dimensions on capacitance change. The substrate thickness is set at 0.5mm in this work to facilitate bending and antenna structure embedding. Nonetheless, Kodak photo paper, Rogers RO 3006, Polyimide, and FR4 were employed as numerical models in this work. Figure 6(a) shows the calculated reactance values together with the varied relative permittivity values used in this investigation. The capacitance is observed to grow dramatically as the p/g is increased. When p/g> 0.5, however, the effect of modifying the permittivity value is seen in a considerable change in the capacitance value. Figure 6(b) shows the S-parameters for solely Kodak photo paper in terms of S11 and S12

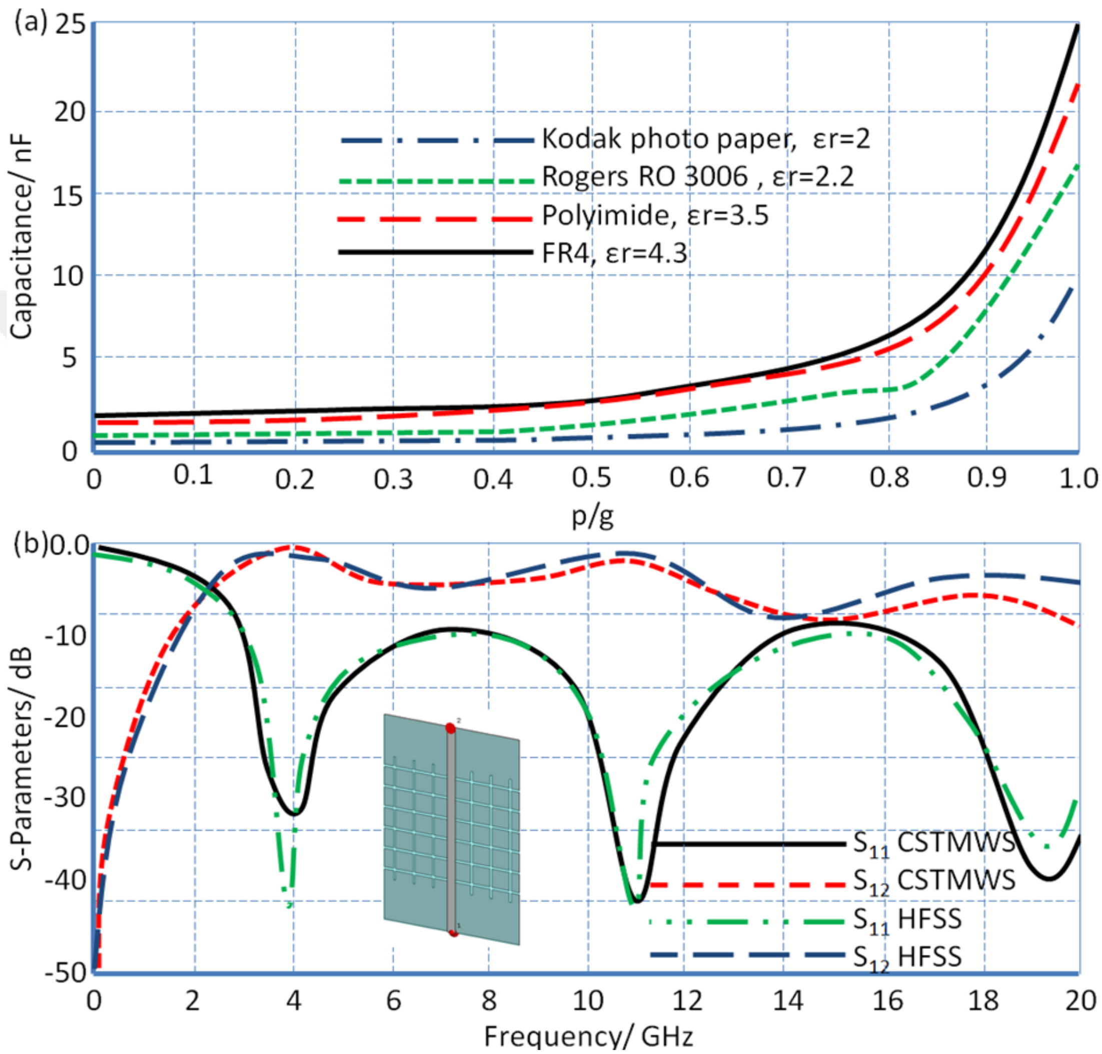

Figure 3.9: EBG characteristics based transmission line structure; (a) Capacitance and (b) S-parameters

4. MEASUREMENTS AND VALIDATIONS

4.1 ANTENNA DESIGN VALIDATION

The numerical results in Fig. 5, S11 spectrum and radiation patterns, are numerically confirmed in this section using HFSS [19]. Figure 6 summarizes the findings of the CST MWS and HFSS simulations. When HSR is applied, the findings of the radiation pattern show that the beam is extremely concentrated. The findings of the software packages employed were found to be extremely well matched

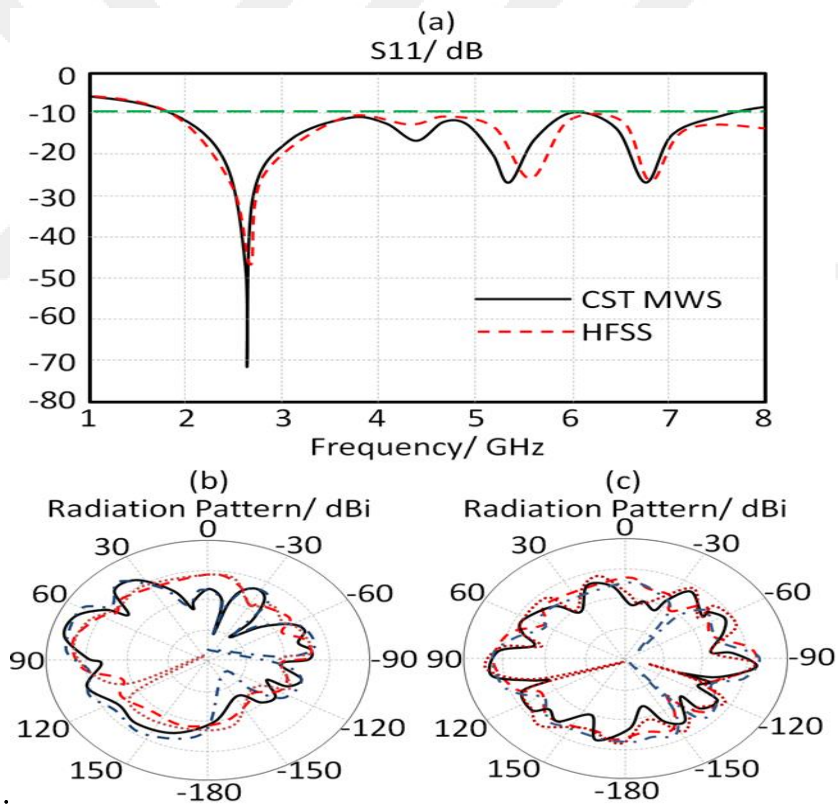

Figure 4.1: Simulated results of the antenna with HSR: (a) S11 spectrum, (b) and (c) Radiation patterns at 2.45 GHz and 5.8 GHz, respectively. Note: The red line for the YX_plane and the black line for the YZ_plane from the CSTMWS. The brown line for the YX_plane and the blue line for the YZ_plane from HFSS

4.2 ANTENNA MEASUREMENTS AND DISCUSSIONS

The constructed prototype, as depicted in Fig.7, is exhibited. To gain good agreement with the simulation findings, the antenna performance is assessed using the HSR construction. Anritsu 37347D Network Analyzer was used to get the observed S11 spectrum (VNA). The radiation patterns within an RF chamber were evaluated using a signal generator.r.

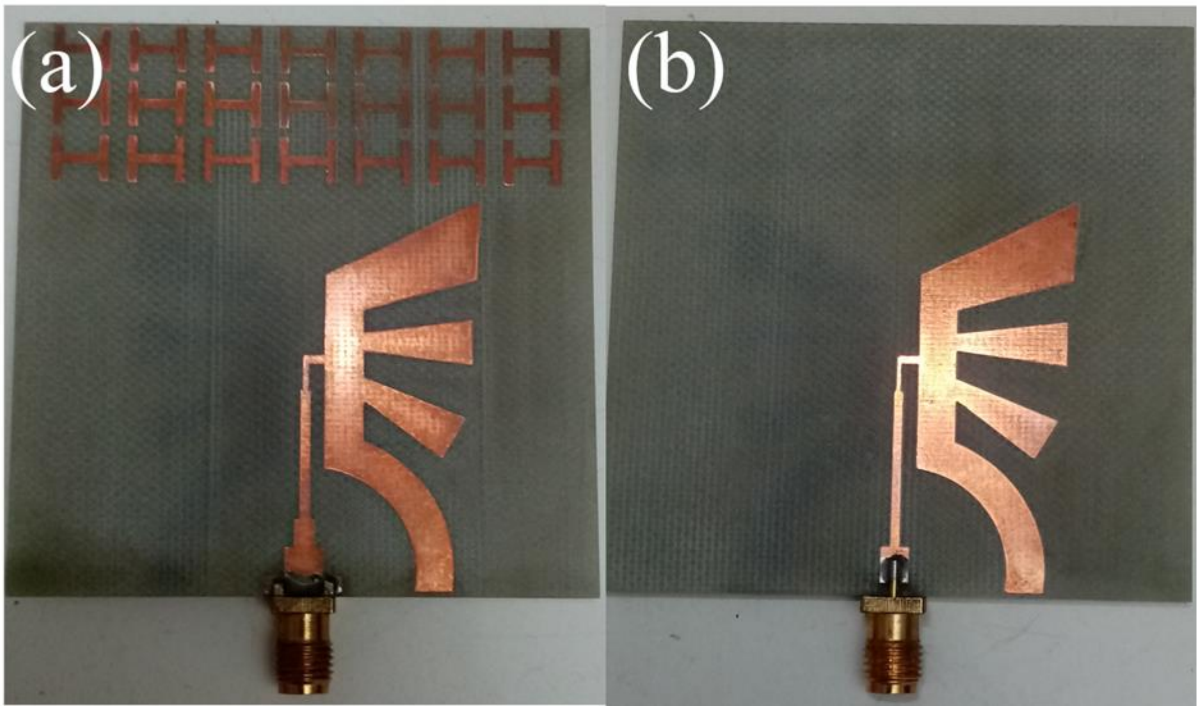

Figure 4.2: Fabricated antenna prototype: (a) Back view and (b) Front view.

As shown in Fig. 8, the suggested, antenna-based HSR structure, has (end-fire) orientation of 2.45 GHz and 5.8 GHz. The antenna's bandwidth ranges start to (1.75 GHz) up to (7.43 GHz). therefore, from(2.45 GHz) to(5.8 GHz,) Nevertheless gain determined to be roughly 9.5 dBi and up to 13 dBi step by step

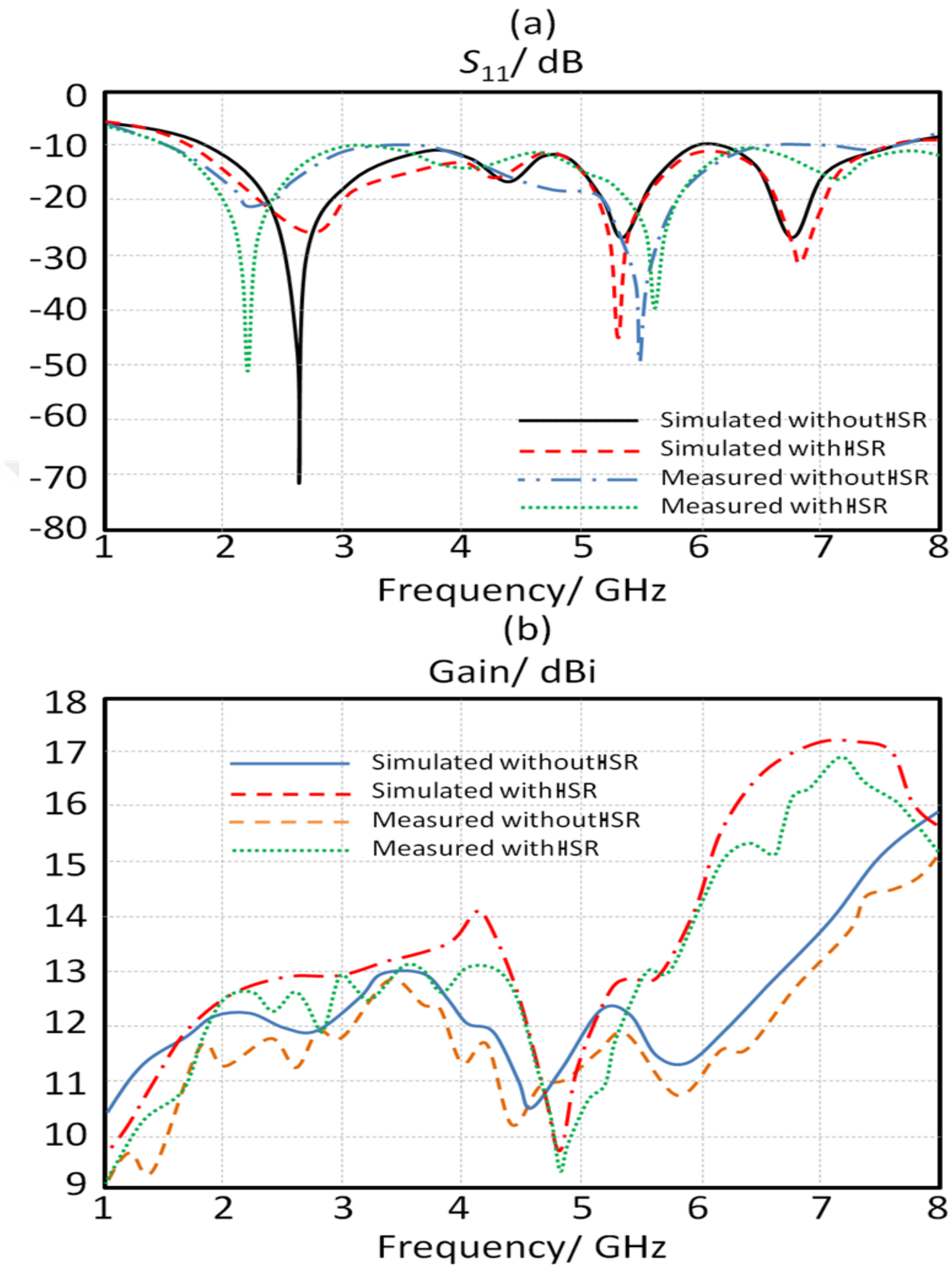

Figure 4.3: Simulated And Measured Antenna Performance: (A) S11 And (B) Gain Spectra.

Fig. 9 The current allocation antennas, both with and without (H), structures. The design with HSR additions contribute, current locomotion to the (patch's) end, hence increasing end-fire gain. In order to extractor the parameters of metamaterial modulation, the most popular and effective method was used. [17].

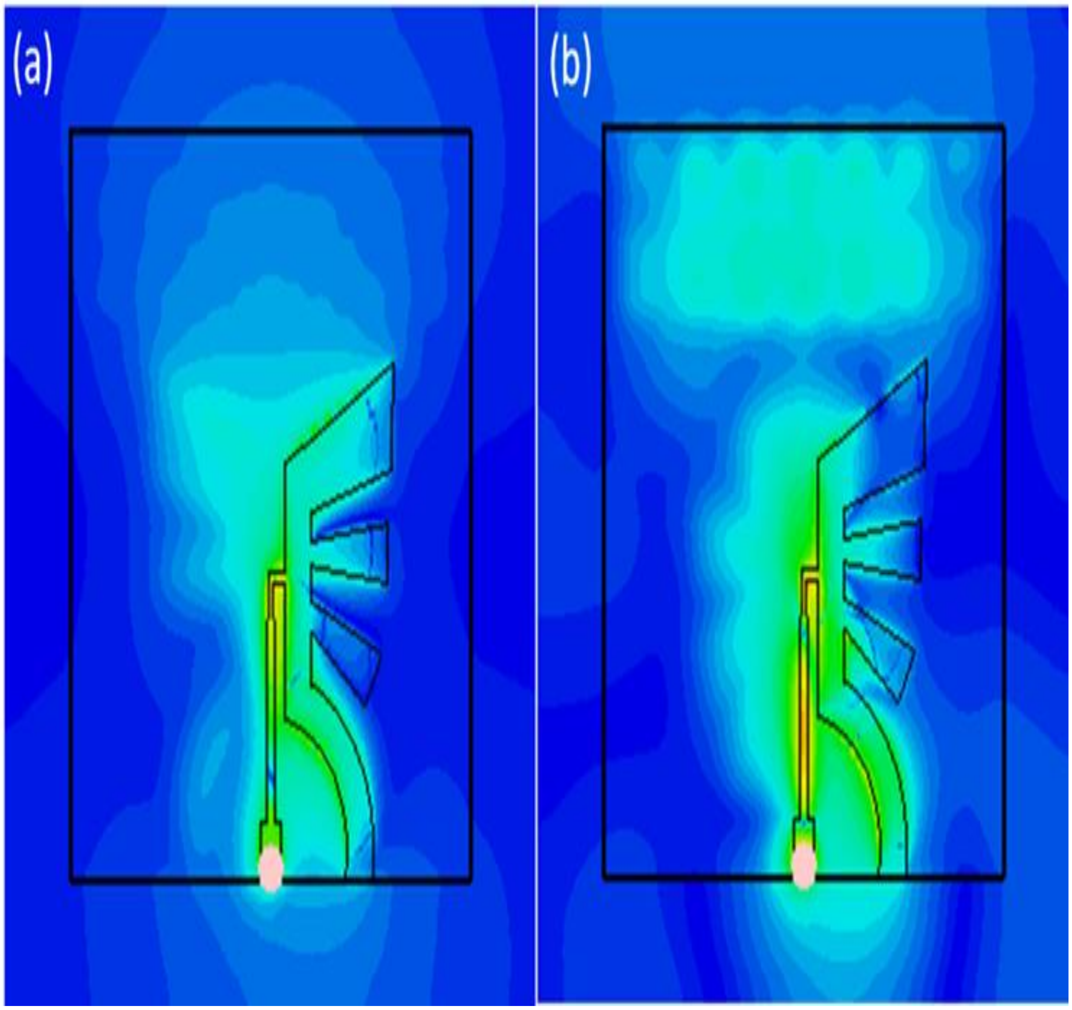

Figure 4.4: Explanation Of The Effect Before And After Adding The HSR

Table 4.1: Comparison for the different published results

Reference	Dimensions (mm^2)	Bandwidth (GHz)	Max. Gain (dBi)
[1]	36×28	2.1GHz-10GHz	4.3
[4]	44×30	1.6GHz-8.5GHz	5.1
[5]	34×32	3.1GHz-10GHz	3.7
[7]	39×38	3GHz-10GHz	4.4
[11]	40×35	2GHz-10GHz	4.7
[15]	70×70	3GHz-12GHz	5.5
[16]	50×63	4.2GHz-6GHz	3.5
[20]	92.5×133	5.5 GHz-6 GHz	10
[21]	185×172	6.52 GHz-6.73 GHz	15.1
Proposed antenna	60×60	1.75 GHz-7.43 GHz	16.71

Table In this paper, I compare a suggested antenna's achievement to different published result.

Table I; Results obtained in comparison to those published

In compared to the published relevant work, the suggested antenna has a greater gain with hight size reduction throughout a wide bandwidth. As a consequence, the suggested antenna is a strong contender against previous published results.

4.3 VINTEGRATION OF A SOLAR PANEL INTO THE PROPOSED ANTENNA DESIGN

In this part, explain after the as a reflector, use a solar panel structure, see Fig. 10(a), to the suggested design performance by eviden (ce s11 digram) and (gain). we do not observe any effect on the antenna radition after adding the solar panel. we can see the simple effect after addition the solar panel on the s11strcture despite of weak effect we notise gain enhanced around 2dB. The solar panel ground plane is made out of metal bus-bars. is responsible for this improvement in gain.The influence of the 0solar panel0 on the, back radiation reflection of the antenna [7]. As a result, has no influence solar panel's, performance.

The antenna gain was a little, enhanced after added the solar panel and to the reflection, back radiation from the ground plane of the (solar panel). The back half of the solar cell is covered with a conductive shield to ensure that all radiation is reflected away from it as shown in F.

It's worth noting that the suggested antenna is positioned on a revolving arm within an RF anechoic room in order to monitor a, radiation patterns. The measuring setup by using horn antenna with a centering lens linked to a vocational Network Analyzer (Agilent PNA 8720) on port 1 and a transmitting antenna with a centering lens. The suggested antenna is attached to the PNA instrument's other port. To secure the far-field region, the antennas are spaced by 4 meters. Radiation patterns and gain spectra are performed using this arrangement. measurements..

The suggested H shape structure array, on the other hand, is used in the research keep the matching impedance mainly constant around 50, as shown in Fig. 11(a), in the real portion and

about 50 in the imaginary part, can be see Fig.11. Nonetheless, as shown in Fig. 1, utilizing the suggestedHSR allowed the antenna radiation efficiency to be practically constant across a wide frequency range. (c).

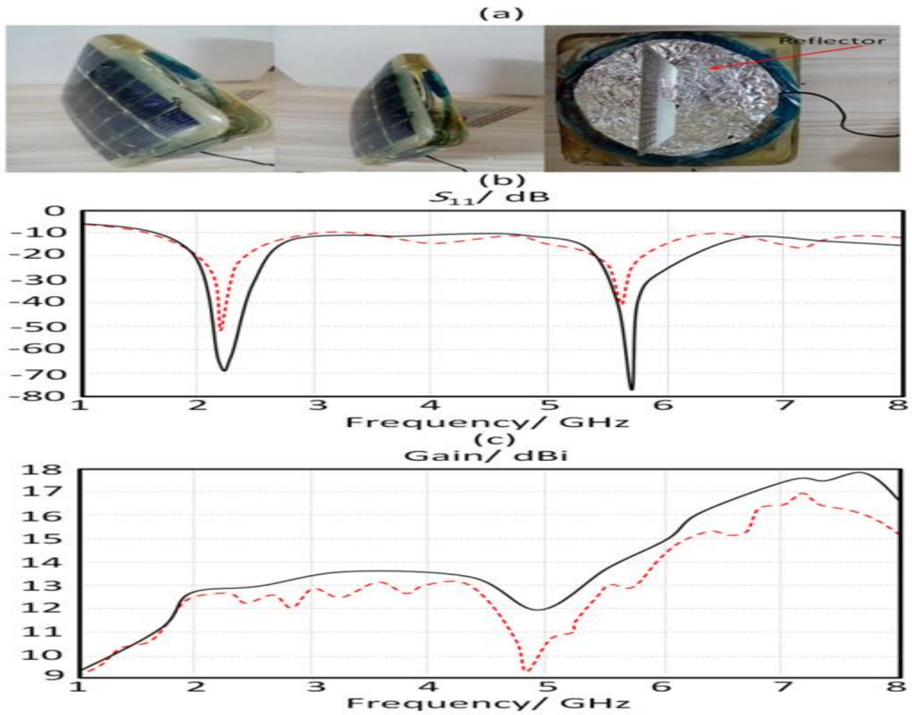

Figure 4.5: Antenna Performance Depending On Reverberatorr Part: (A) Solar Panel Antenna Construction, (B) S Parameters, (C) Gain Note: The Measurements Without The Solar Panel Are Indicated By The Red Dotted Line. The Measurements With The Solar Panel Are Represented By The Black Solid Line.

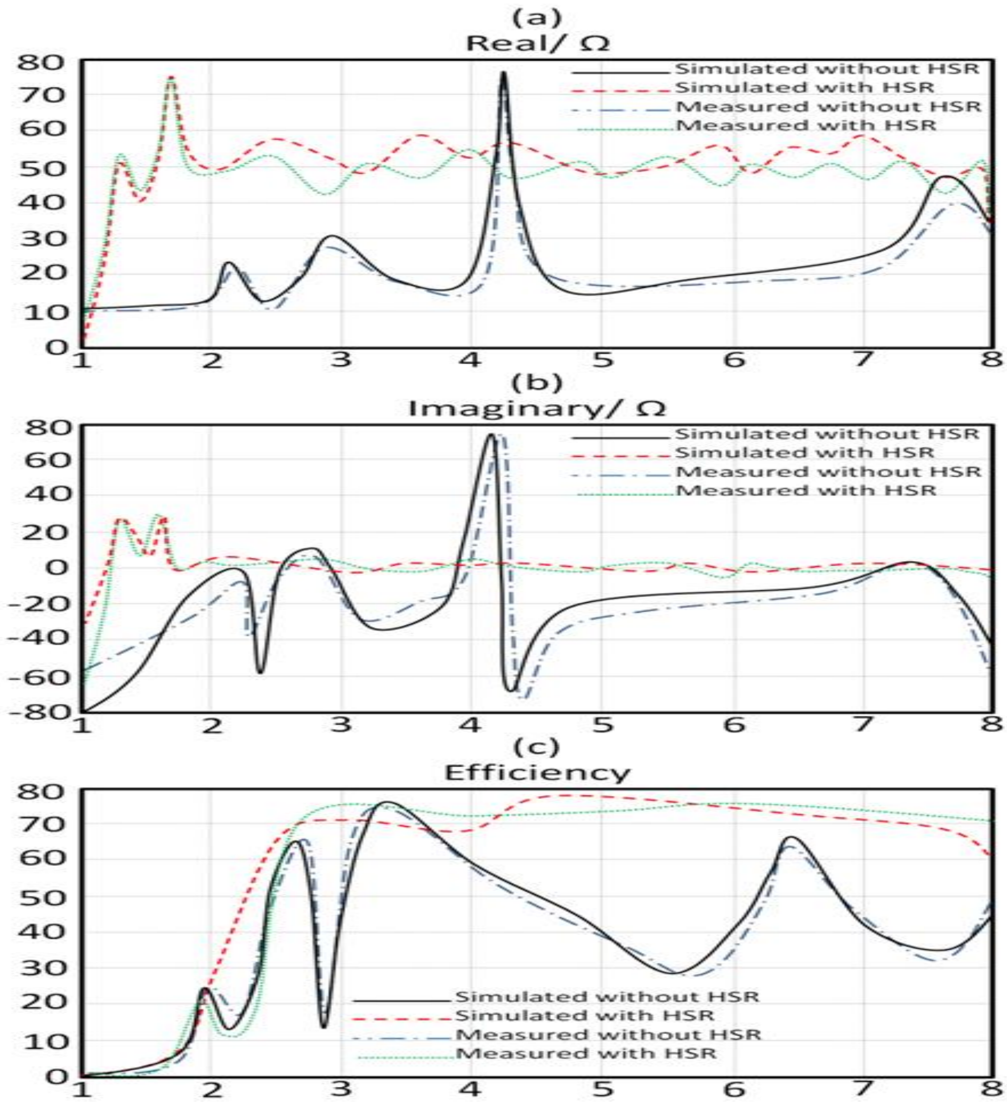

Figure 4.6: Antenna Performance With And Without The Proposed HSR: (A) Real Part Of The Impedance, (B) Imaginary Part Of The Impedance, (C) Radiation Efficiency Spectra.

It is clear that the suggested solar panel's material losses have no substantial impact on antenna efficiency since the antenna was mounted perpendicular, to a solar panel, keeping the radiation of antenna far for the (solar panel).

After the added antenna is installed, a 1-V characteristics of the solar panels are now measured. This comparison is used to determine the consequences of the antenna installation on the sub solar panel. As a result, minimal impacts by solar panel execution, are discovered; see Fig. 12 after, and before, the antenna insert. that s effect by the antenna construction being located on the solar panel's rear panel. At varied light intensities, the solar energy is defined in the (photo-current) , (photo-voltage) diagram by altering the value from 500W/m2 to 1000W/m2 as presented in Fig. 12.

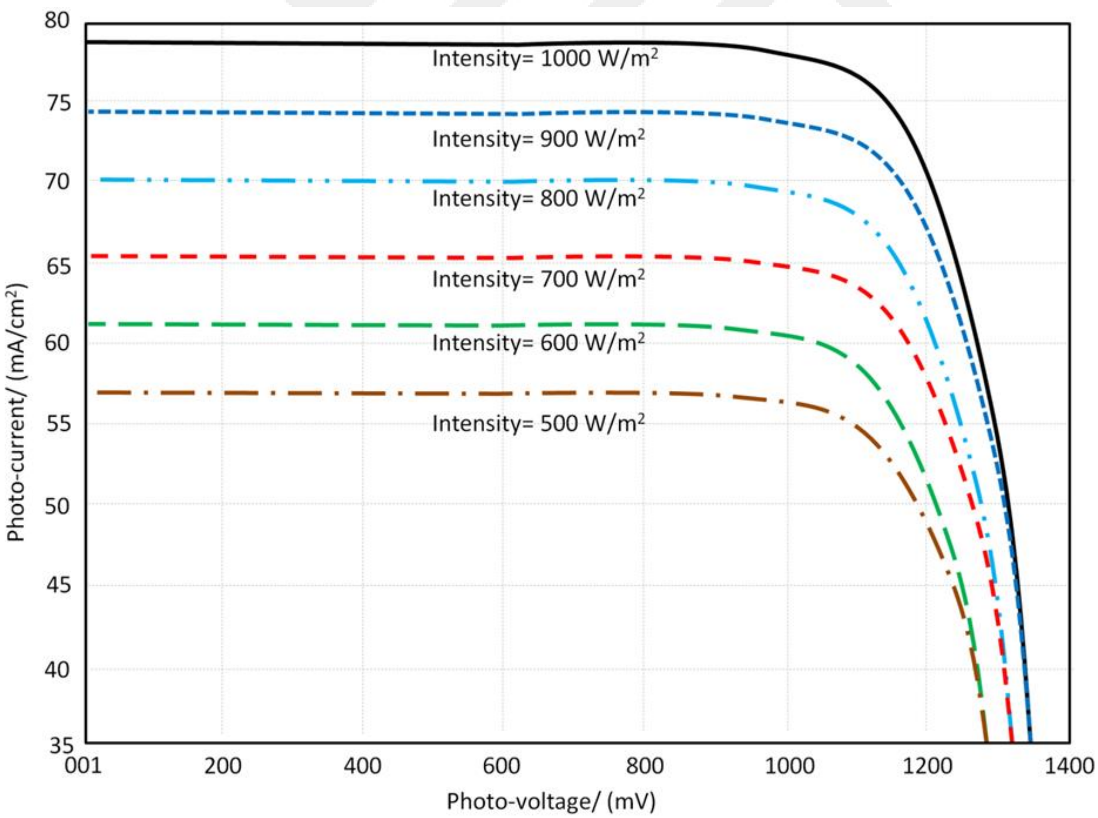

Figure 4.7: After implementing the proposed antenna configuration to the rear panel, a solar panel performance improved.

5. CONCLUSION AND FUTURE WORK

5.1 CONCLUSION

The concept of employing a UWB Vivaldi fractal antenna for the RF harvesting is investigated in depth based on analytical and computational investigations backed by experimental validations in this study. A microstrip patch with Sierpinski triangle fractal slots will be used to make the suggested antenna. For antenna bandwidth augmentation, the patch structure is supplied with a flared CPW with a flared matching circuit. To improve antenna radiation efficiency, a partial continuous layer defective with EBG pads is proposed as the antenna ground plane. When coupled to a full wave bridge rectifier board for RF harvesting, the proposed antenna is tested. This study shows a high gain broadband microstrip antenna with HSR features for self-powered wireless systems in the Wi-Fi spectrum. Broadband is obtained by matching the antenna bandwidth, |S11|-10 dB, from 1.75 GHz to 7.43 GHz, using a microstrip-to-stripline transition balun. The gain improvement is related to the use of the HSR array, which has a range of 9.52 dBi to 16.71 dBi throughout the full frequency spectrum. The gain enhancement is attributed for employing HSR array to be ranged between 9.52 dBi and 16.71 dBi within the entire frequency band. When comparing the suggested antenna to the different published it is discovered that the fabrisated antenna delivers significant gains, bandwidth, and size decreasing. When the suggested antenna is put on a solar panel as a reflector, nevertheless, it is discovered that the achievementof the antenna in terms of S11 spectra is unaffected, but the antenna gain is increased in general throughout the whole frequency spectrum of inters. For that reason the structure of the antenna is linked to the rear panel of the solar energy, the achievement of the

employed solar panel is assessed in terms of I-V discriminatory,to indicate no detrimental impacts on solar energy harvesting. Lastly, the simulated and measured findings were found to accord quite well.

5.2 FUTURE WORK

A study was used by the author. on developing a printed circuit antenna for RF harvesting at various frequency bands in this work, however, there will be a lot more development in the future. that may be subjected to further investigation, such as the following:

a. The layout that has been proposed is implemented using a FR-4 substrate. However, the author intends to do further research on a foldable solar panel to provide a dual charging source in the future.

b. The suggested antenna is produced using a copper layer etched from an FR4 substrate; however, the printing is used technique based nanoscale ink that is conductive build the fabrected antenna is a subject for future research.

c. As a result of the author's use of a third-order fractal structure, the object, of this research in the future will be to apply additional orders.

d. Because the antenna is supplied with a quarter wavelength transformer to achieve good matching impedance, a second transformer may be required in the future.

e. In a future research, the circuit rectifier design will be used to the antenna design.

f. The antenna is designed to support two frequency bands; however, the author hopes to expand the antenna design in the future to support an ultra- wide band matching bandwidth over more frequency bands.

REFERENCES

[1] B. S. Bashar, M. M. Ismail, and A.-S. M. Talib, "Optimize Cellular Network Performance Using Phased Arrays," in IOP Conference Series: Materials Science and Engineering, 2020, vol. 870, no. 1: IOP Publishing, p. 012128.

[2] R. Vincenti Gatti, R. Rossi, and M. Dionigi, "Single-Layer Line-Fed Broadband Microstrip Patch Antenna on Thin Substrates," Electronics, vol. 10, no. 1, p. 37, 2021.

[3] F. J. Magalhaes and D. B. Oliveira, "Design of low-cost microstrip patch antennas with robust optimization," Journal of Electromagnetic Waves and Applications, vol. 35, no. 4, pp. 454-465, 2021.

[4] A. S. Gaid, A. M. Alhakimi, O. Y. Sae'ed, M. S. Alasadee, and A. A. Ali, "Compact and bandwidth efficient multi-band microstrip patch antennas for 5G applications," in International Conference of Reliable Information and Communication Technology, 2019: Springer, pp. 663-672.

[5] R. Waterhouse, "Microstrip patch antennas," in Handbook of Antennas in Wireless Communications: CRC Press, 2018, pp. 6-1-6-27.

[6] V. Prakasam, P. Sandeep, and K. A. LaxmiKanth, "Design and Analysis of Rectangular Microstrip Patch Antenna for 2.4 GHz Wireless Communication Applications Using CST Microwave Studio," in Computer Networks and Inventive Communication Technologies: Springer, 2021, pp. 1113-1125.

[7] M. A. Al-Amoudi, "Study, Design, and Simulation for Microstrip Patch Antenna," International Journal of Applied Science and Engineering Review (IJASER), vol. 2, no. 2, pp. 1-29, 2021.

[8] J. Anguera, A. Andújar, and J. Jayasinghe, "High-directivity microstrip patch antennas based on TM odd-0 modes," *IEEE Antennas and Wireless Propagation Letters, vol. 19, no. 1, pp. 39-43, 2019.*

[9] K. Da Xu, H. Xu, Y. Liu, J. Li, and Q. H. Liu, "Microstrip patch antennas with multiple parasitic patches and shorting vias for bandwidth enhancement," *IEEE Access, vol. 6, pp. 11624-11633, 2018.*

[10] M. A. K. Khan, T. A. Shaem, and M. A. Alim, "Graphene patch antennas with different substrate shapes and materials," Optik, vol. 202, p. 163700, 2020.

[11] S. K. Danasegaran, E. C. Britto, and S. C. Xavier, "Exploration of Trigonal Patch Antenna Characteristics with the Impact of 2D Photonic Crystal of Various Air Hole Shapes," Journal of Electronic Materials, vol. 50, no. 9, pp. 5365-5374, 2021.

[12] Y. S. Mezaal, "New compact microstrip patch antennas: Design and simulation results," Indian Journal of Science and Technology, vol. 9, no. 12, pp. 1-6, 2016.

[13] A. Kumar, N. Gupta, and P. Gautam, "Gain and bandwidth enhancement techniques in microstrip patch antennas-a review," International Journal of Computer Applications, vol. 148, no. 7, 2016.

[14] D. V. Prakasam and D. P. Sandeep, "Different Feeding Techniques of Elliptical Patch Antenna at X Band for Radar Applications," International Journal of Computing and Digital Systems, vol. 10, 2021.

[15] A. Bharathi, L. Merugu, and P. Somasekhar Rao, "Reconfigurable corner truncated square microstrip patch antennas for wireless communication applications," IETE Journal of Research, vol. 66, no. 2, pp. 242-255, 2020.

[16] X. Liu et al., "A Wideband Triple-Mode Differentially-Fed Microstrip Patch Antenna," *IEEE Antennas and Wireless Propagation Letters, 2021*.

[17] X. Zhang, K.-D. Hong, L. Zhu, X.-K. Bi, and T. Yuan, "Wideband differentially fed patch antennas under dual high-order modes for stable high gain," IEEE Transactions on Antennas and Propagation, vol. 69, no. 1, pp. 508-513, 2020.

[18] M. M. Shirkolaei and M. Jafari, "A new class of wideband microstrip falcate patch antennas with reconfigurable capability at circular- polarization," Microwave and Optical Technology Letters, vol. 62, no. 12, pp. 3922-3927, 2020.

[19] Z. Shao, L.-F. Qiu, and Y. P. Zhang, "Design of wideband differentially fed multilayer stacked patch antennas based on bat algorithm," *IEEE Antennas and Wireless Propagation Letters, vol. 19, no. 7, pp. 1172-1176, 2020.*

[20] M. Y. Sai, S. Kavya, S. R. Bhimavarapu, M. Mudaliar, and S. Sharma, "CPW Fed Microstrip Patch Antenna for Dedicated Short-Range Communication," Wireless Personal Communications, pp. 1-15, 2021.

[21] P. Kuchhal, H. Castillo, R. G. Mishra, and R. Mishra, "Design and Analysis of a Dual-Band CPW fed Microstrip Patch Antenna," in 2021 5th International Conference on Computing Methodologies and Communication (ICCMC), 2021: IEEE, pp. 53-60.

[22] R. Tiwari, A. Bagwari, and V. S. Kushwah, "Parameter improvement of micro strip patch antennas using various techniques: A review," Materials Today: Proceedings, vol. 29, pp. 492-500, 2020.

[23] C. M. Preddy, R. Singh, P. H. Aaen, and S. R. P. Silva, "Integrated Carbon-Fiber-Reinforced Plastic Microstrip Patch Antennas," *IEEE Antennas and Wireless Propagation Letters, vol. 19, no. 4, pp. 606-610, 2020.*

[24] Z. N. Chen, "Metantennas: From Patch Antennas to Metasurface Mosaic Antennas," in 2020 IEEE Asia-Pacific Microwave Conference (APMC), 2020: IEEE, pp. 363-365.

[25] J. Zeng, X. Liang, L. He, F. Guan, F. H. Lin, and J. Zi, "Single-Fed Triple-Mode Wideband Circularly Polarized Microstrip Antennas Using Characteristic Mode Analysis," IEEE Transactions on Antennas and Propagation, 2021.

[26] A. P. Ambalgi, S. Sujata, U. Mamodiya, and P. Sharma, "Effects of Single and Double Wide Slots on Microstrip Patch Antennas Characteristics Using Direct Contact Probe Feed Excitation with Broadsided Radiation," in Proceedings of Second International Conference on Smart Energy and Communication, 2021: Springer, pp. 423-432.

[27] V. Prakasam and N. Reddy, "Design and simulation of elliptical micro strip patch antenna with coaxial probe feeding for satellites applications using matlab," in 2020 Fourth International Conference on I-SMAC (IoT in Social, Mobile, Analytics and Cloud)(I-SMAC), 2020: IEEE, pp. 228-234.

[28] A. Bansal and R. Gupta, "A review on microstrip patch antenna and feeding techniques," International Journal of Information Technology, vol. 12, no. 1, pp. 149-154, 2020.

[29] H. Nawaz and I. Tekin, "Dual-polarized, differential fed microstrip patch antennas with very high interport isolation for full-duplex communication," IEEE transactions on antennas and propagation, vol. 65, no. 12, pp. 7355-7360, 2017.

[30] M. A. Kumar, K. Rameshchandra, and S. Bachu, "FRCAPE: Frequency Re-configurable Co-planar Antenna Using Parasitic Elements," in 2020 IEEE International Conference on Advent Trends in Multidisciplinary Research and Innovation (ICATMRI), 2020: IEEE, pp. 1-5.

[31] A. Srivastava et al., "Microstrip rectangular patch antenna using coplanar parasitic rod elements with substrate integrated feeding line technique," J. Math. Comput. Sci., vol. 11, no. 4, pp. 5071-5082, 2021.

[32] S. P. Pinapati, J. Brittain, A. Caldow, and C. Fumeaux, "Wearable textile EBG-inspired bandwidth-enhanced patch antenna," IET Microwaves, Antennas & Propagation, vol. 14, no. 15, pp. 2011-2019, 2020.

[33] L. Zou, X. Wang, W. Wang, and H. Gao, "Ka-band microstrip array antenna with compact series-parallel hybrid strip-line feeding network," IEICE Electronics Express, vol. 18, no. 14, pp. 20210231-20210231, 2021.

[34] H. M. Al-Sabbagh, T. A. Elwi, Y. Al-Naiemy, and H. M. Al-Rizzo, “A Compact Triple-Band Metamaterial-Inspired Antenna for Wearable Applications”, Microwave and Optical Technology Letters, Volume 11, number 2, October 2019,

[35] M. Piñuela, P. D. Mitcheson, and S. Lucyszyn, “Ambient RF energy harvesting in urban and semi-urban environments,” IEEE Trans. Microw. Theory Techn., vol. 61, no. 7, pp. 2715–2726, Jul. 2013,

[36] C. Song et al., “A novel six-band dual CP rectenna using improved impedance matching technique for ambient RF energy harvesting,” IEEE Trans. Antennas Propag., vol. 64, no. 7, pp. 3160–3171, Jul. 2016,

[37] S. Shen and R. D. Murch, “Designing dual-port pixel antenna for ambient RF energy harvesting using genetic algorithm,” IEEE International Symposium on Antennas and Propagation USNC/URSI National Radio Science Meeting, Jul. 2015, pp. 1286–1287, in 2015

[38] S. Shen, C.-Y. Chiu, and R. D. Murch, “Multiport pixel rectenna for ambient RF Energy Harvesting,” IEEE Transactions on Antennas and Propagation, vol. 66, no. 2, pp. 644–656, 2018.

[39] S. Shen, C. Y. Chiu, and R. D. Murch, “A dual-port triple-band L-probe microstrip patch rectenna for ambient RF energy harvesting,” *IEEE Antennas Wireless Propag. Lett., vol. 16, pp. 3071–3074, 2017,*

[40] S. Shen, Y. Zhang, C. Y. Chiu, and R. D. Murch, “A compact quad-port dual-polarized dipole rectenna for ambient RF energy harvesting,” in 2018 12th European Conference on Antennas and Propagation (EUCAP), London, Apr. 2018,

[41] S. Shen, Y. Zhang, C. Y. Chiu, and R. Murch, “An ambient RF energy harvesting system where the number of antenna ports is dependent on frequency,” IEEE Trans. Microw. Theory Techn., 2019, accepted

[42] U. Olgun, C.-C. Chen, and J. L. Volakis, “Investigation of rectenna arrayconfigurations for enhanced RF power harvesting,” IEEE Antennas Wireless Propag. Lett., vol. 10, pp. 262–265, 2011,

[43] J. A. Hagerty, F. B. Helmbrecht, W. H. McCalpin, R. Zane, and Z. B. Popovic, “Recycling ambient microwave energy with broad-band rectenna arrays,” *IEEE Trans. Microw. Theory Techn., vol. 52, no. 3, pp. 1014–1024, Mar. 2004,*

[44] T. S. Almoneef, H. Sun, and O. M. Ramahi, “A 3-D folded dipole antenna array for far-field electromagnetic energy transfer,” *IEEE Antennas Wireless Propag. Lett., vol. 15, pp. 1406–1409, 2016,*

[45] S. Shen and R. D. Murch, “Impedance matching for compact multiple antenna systems in random RF fields,” *IEEE Trans. Antennas Propag., vol. 64, no. 2, pp. 820–825, Feb. 2016,*

[46] S. Soltani and R. D. Murch, “A compact planar printed MIMO antenna design,” IEEE Trans. Antennas Propag., vol. 63, no. 3, pp. 1140–1149, Mar. 2015,

[47] S. Shen, Y. Sun, S. Song, D. P. Palomar, and R. D. Murch, “Successive Boolean optimization of planar pixel antennas,” *IEEE Trans. Antennas Propag., vol. 65, no. 2, pp. 920–925, Feb. 2017*

[48] A. R. Azeez, T. A. Elwi and Z. A. Abed AL-Hussain, "A Numerical Study of the Antipodal Vivaldi Antenna Design for Ultra-Wideband Applications", SAUSSUREA Multidisciplinary International Peer Reviewed Journal, **v**olume 6, no. 5, pp. 366-370, August 201**6**,

[49] T. A. Elwi, A. I. Imran, and Y. Alnaiemy, "A Miniaturized Lotus Shaped Microstrip Antenna Loaded with EBG Structures for High Gain-Bandwidth Product Applications", Progress In Electromagnetics Research C**, v**olume 60, pp. 157-167, December 201**5,**

[50] T. A. Elwi, M. M. Hamed, Z. Abbas, and M. A. Elwi, “On the Performance of the 2D Planar Metamaterial Structure”, International Journal of Electronics and Communications, volume 68, issue 9, pp. 846–850, September 2014,

[51] T. Elwi, “No frequency reuse: Wearable steerable MIMO microstrip antenna array for mobile ad hoc applications,” British Journal of Applied Science & Technology, vol. 4, no. 17, pp. 2477–2488, 2014.

[52] T. A. Elwi, M. Noori, Y. Al-Naiemy, Ethaitr S. Yahiea, "Conformal Antenna Array for MIMO Applications", Journal of Electromagnetic Analysis and Applications, volume 6, pp. 43-50, March 2014,

[53] T. A. Elwi, H. M. Al-Rizzo, D. G. Rucker, and H. R. Khaleel, **"**Effects of twisting and bending on the performance of a miniaturized truncated sinusoidal printed circuit antenna for wearable biomedical telemetry devices," AEU - International Journal of Electronics and Communications, volume 13, no. 1, pp 1-12, March 2010,

[54] T. A. Elwi, "Metamaterial based a printed monopole antenna for sensing applications," International Journal of RF and Microwave Computer-Aided Engineering, vol. 28, no. 7, 2018.

[55] H. S. Ahmed and T. A. Elwi, "SAR Effects Reduction Using Reject Band Filter Arrays for Wi-Fi Portable Devices", International Journal of Electronics Letters, Taylor & Francis, volume 9, issue 12, May 2018,

[56] T. A. Elwi, "A Slotted Lotus Shaped Microstrip Antenna based an EBG Structure", Journal of Material Sciences & Engineering, volume 7, issue 2, March 2018,

[57] "Ansys HFSS | 3D High Frequency Simulation Software", Ansys.com, 2022. [Online]. Available: https://www.ansys.com/products/electronics/ansys-hfss. [Accessed: 06- Sep-2022].

[58] [12]2022. [Online]. Available: http://www.matlab.com/. [Accessed: 06- Sep- 2022].

[59] [14]"AnvSoft - Video Converter, Video Enhancer AI, Audio Converter, Android & iOS Mobile Manager, Photo DVD Maker, PDFMate Converter", Anvsoft.com, 2022. [Online]. Available: https://anvsoft.com/. [Accessed: 06- Sep- 2022].

[60] S. Shen, C.-Y. Chiu, and R. D. Murch, "A Broadband L-probe microstrip patch rectenna for ambient RF Energy Harvesting," 2017 IEEE International Symposium on Antennas and Propagation & USNC/URSI National Radio Science Meeting, 2017.

[61] "CST - Computer Simulation Technology - Crunchbase Company Profile & Funding," Crunchbase. [Online]. Available: https://www.crunchbase.com/organization/cst-computer-simulation-technolog. [Accessed: 06-Sep-2022].